Structure-preserving tangential interpolation for model reduction of port-Hamiltonian systems

Gugercin, Serkan; Polyuga, Rostyslav V.; Beattie, Christopher; Schaft, Arjan van der

Published in:
Automatica

DOI:
10.1016/j.automatica.2012.05.052

Publication date:
2012

Automatica 48 (2012) 1963–1974

Contents lists available at SciVerse ScienceDirect

Automatica

journal homepage: www.elsevier.com/locate/automatica

Structure-preserving tangential interpolation for model reduction of port-Hamiltonian systems☆

Serkan Gugercin [a,1], Rostyslav V. Polyuga [b], Christopher Beattie [a], Arjan van der Schaft [c]

[a] Department of Mathematics, Virginia Tech, Blacksburg, VA 24061-0123, USA

[b] ABN AMRO N.V. Bank, Gustav Mahlerlaan 10, 1082 PP (PAC HQ2015) Amsterdam, The Netherlands

[c] Johann Bernoulli Institute for Mathematics and Computer Science, University of Groningen, P.O. Box 407, 9700 AK Groningen, The Netherlands

ARTICLE INFO

Article history:
Received 17 January 2011
Received in revised form
20 December 2011
Accepted 16 February 2012
Available online 12 July 2012

Keywords:
Model reduction
Interpolation
Port-Hamiltonian systems
Structure preservation
$\mathcal{H}_2$ approximation

ABSTRACT

Port-Hamiltonian systems result from port-based network modeling of physical systems and are an important example of passive state-space systems. In this paper, we develop a framework for model reduction of large-scale multi-input/multi-output port-Hamiltonian systems via tangential rational interpolation. The resulting reduced model is a rational (tangential) interpolant that retains the port-Hamiltonian structure; hence it remains passive. We introduce an $\mathcal{H}_2$-inspired algorithm for effective choice of interpolation points and tangent directions and present several numerical examples illustrating its effectiveness.

1. Introduction

Port-based network modeling (The Geoplex Consortium, 2009) exploits the common circumstance that the system under study is decomposable into subsystems which are interconnected through (vector) pairs of variables whose product gives the power exchanged among subsystems. This approach is especially useful for multi-physics systems, where subsystems may be associated with different categories of physical phenomena (e.g., mechanical, electrical, or hydraulic). This leads to consideration of *port-Hamiltonian* system representations (see The Geoplex Consortium, 2009, van der Schaft, 2000a,b and van der Schaft & Maschke, 1995 and references therein) which encode structural features related to the manner in which energy is distributed and across subsystems.

Models of complex physical systems often involve discretized systems of coupled partial differential equations which lead immediately to dynamic models having very large state-space dimension. This creates a need for *model reduction* methods capable of producing (comparatively) low dimension surrogate models that are able to mimic closely the original system's input/output map. It is highly desirable for the reduced model also to preserve port-Hamiltonian structure when present in the original system, so as to maintain a variety of system properties, such as energy conservation and passivity.

Preservation of port-Hamiltonian structure in the reduction of large scale port-Hamiltonian systems has been considered in Polyuga and van der Schaft (2008, 2010a, 2011b) using Gramian-based methods; we briefly review one such approach in Section 3.1. For the special case of a single-input/single-output (SISO) system, the use of (rational) Krylov methods was employed in Gugercin, Polyuga, Beattie, and van der Schaft (2009), Polyuga and van der Schaft (2010b, 2011a) and Wolf, Lohmann, Eid, and Kotyczka (2010). In particular, (Polyuga & van der Schaft, 2010b, 2011a; Wolf et al., 2010) all deal with system interpolation at single points only. In this work, we develop multi-point rational tangential interpolation of multi-input/multi-output (MIMO) port-Hamiltonian systems. Preservation of port-Hamiltonian structure by reducing the underlying full-order Dirac structure was presented in Polyuga and van der Schaft (2012) and van der Schaft and Polyuga (2009). A perturbation approach is considered in Hartmann (2009) and Hartmann, Vulcanov, and Schütte (2010). See Polyuga (2010) for an overview of recent port-Hamiltonian model reduction methods.

☆ The work of SG has been supported in part by NSF Grant DMS-0645347. The material in this paper was not presented at any conference. This paper was recommended for publication in revised form by Associate Editor Fen Wu under the direction of Editor Roberto Tempo.

E-mail addresses: gugercin@math.vt.edu (S. Gugercin), rostyslav.polyuga@gmail.com (R.V. Polyuga), beattie@vt.edu (C. Beattie), A.J.van.der.Schaft@rug.nl (A. van der Schaft).

[1] Tel.: +1 540 231 6549; fax: +1 540 231 5960.

0005-1098/$ – see front matter © 2012 Elsevier Ltd. All rights reserved.
doi:10.1016/j.automatica.2012.05.052

For general MIMO dynamical systems, interpolatory model reduction methods produce reduced models whose transfer functions interpolate the original system transfer function at selected points in the complex (frequency) plane along selected input/output directions. The main implementation cost involves solving (typically sparse) linear systems, giving a significant advantage in large-scale settings over competing Gramian-based methods (such as balanced truncation) that must contend with a variety of large-scale dense matrix operations. Indeed, a Schur decomposition is required for computing *exact* Gramians but recent advances using ADI-type algorithms allow iterative computation of *approximate* Gramians in large-scale settings; see, for example, Benner, Quintana-Ortí, and Quintana-Ortí (2003), Freitas, Rommes, and Martins (2008), Gugercin, Sorensen, and Antoulas (2003), Heinkenschloss, Sorensen, and Sun (2008), Penzl (2000), Sabino (2007), Sorensen and Antoulas (2002), Stykel (2004) and references therein.

Until recently, there were no systematic strategies for selecting interpolation points and directions, but this was largely resolved by Gugercin (2005) and Gugercin, Antoulas, and Beattie (2006, 2008) who proposed an interpolatory model reduction strategy leading to $\mathcal{H}_2$-optimal reduced models. See Bunse-Gerstner, Kubalinska, Vossen, and Wilczek (2010), Kubalinska, Bunse-Gerstner, Vossen, and Wilczek (2007) and Van Dooren, Gallivan, and Absil (2008) for related work and Antoulas, Beattie, and Gugercin (2010) for a recent survey.

In this paper, we demonstrate that interpolatory model reduction for linear state-space systems can be applied to MIMO port-Hamiltonian systems so as to preserve *port-Hamiltonian structure* in the reduced models, preserving as a consequence *passivity* as well. We introduce a numerically efficient $\mathcal{H}_2$-based algorithm for structure-preserving model reduction of port-Hamiltonian systems that produces high quality reduced models in general MIMO cases. Numerical examples are presented to illustrate the effectiveness of the method.

We review in Section 2 the solution to the rational tangential interpolation problem for general linear MIMO systems. A brief theory on port-Hamiltonian systems is given in Section 3. Structure-preserving interpolatory model reduction of port-Hamiltonian systems in different coordinates is considered in Section 4 where we show theoretical equivalence of interpolatory reduction methods using different coordinate representations of port-Hamiltonian systems and discuss which is most robust and numerically effective. $\mathcal{H}_2$-based model reduction for port-Hamiltonian systems together with the proposed algorithm is presented in Section 5 followed by numerical examples in Section 6.

2. Interpolatory model reduction

Let $\mathbf{G}$ be a dynamical system with state-space realization given as

$$\mathbf{G}: \begin{cases} \mathbf{E}\dot{\mathbf{x}}(t) = \mathbf{A}\mathbf{x}(t) + \mathbf{B}\mathbf{u}(t) \\ \mathbf{y}(t) = \mathbf{C}\mathbf{x}(t), \end{cases} \tag{1}$$

where $\mathbf{A}, \mathbf{E} \in \mathbb{R}^{n\times n}$, $\mathbf{E}$ is nonsingular, $\mathbf{B} \in \mathbb{R}^{n\times m}$, and $\mathbf{C} \in \mathbb{R}^{p\times n}$. For each t, $\mathbf{x}(t) \in \mathbb{R}^n$, $\mathbf{u}(t) \in \mathbb{R}^m$, and $\mathbf{y}(t) \in \mathbb{R}^p$ denotes, respectively, the *state*, *input*, and *output* of $\mathbf{G}$. The Laplace transform of (1) leads to the associated transfer function $\mathbf{G}(s) = \mathbf{C}(s\mathbf{E}-\mathbf{A})^{-1}\mathbf{B}$. Following the usual convention, the underlying dynamical system and its transfer function are both denoted by $\mathbf{G}$.

We wish to produce a surrogate dynamical system $\mathbf{G}_r$ of much smaller order with a similar state-space form

$$\mathbf{G}_r: \begin{cases} \mathbf{E}_r\dot{\mathbf{x}}_r(t) = \mathbf{A}_r\mathbf{x}_r(t) + \mathbf{B}_r\mathbf{u}(t) \\ \mathbf{y}_r(t) = \mathbf{C}_r\mathbf{x}_r(t), \end{cases} \tag{2}$$

where $\mathbf{A}_r, \mathbf{E}_r \in \mathbb{R}^{r\times r}$, $\mathbf{B}_r \in \mathbb{R}^{r\times m}$, and $\mathbf{C}_r \in \mathbb{R}^{p\times r}$ with $r \ll n$ such that the reduced system output, $\mathbf{y}_r(t)$, approximates the original system output, $\mathbf{y}(t)$, with high fidelity as measured with respect to the $\mathcal{H}_2$ norm. This will be discussed in some detail in Sections 2.2 and 5.

We construct reduced models via Petrov–Galerkin projections: two r-dimensional subspaces $\mathcal{V}_r$ and $\mathcal{W}_r$ are chosen with associated basis matrices $\mathbf{V}_r \in \mathbb{R}^{n\times r}$ and $\mathbf{W}_r \in \mathbb{R}^{n\times r}$ ($\mathcal{V}_r = \text{Range}(\mathbf{V}_r)$ and $\mathcal{W}_r = \text{Range}(\mathbf{W}_r)$). Then system dynamics are approximated by approximating the full-order state $\mathbf{x}(t) \approx \mathbf{V}_r\mathbf{x}_r(t)$ and forcing

$$\begin{aligned} &\mathbf{W}_r^T\left(\mathbf{E}\mathbf{V}_r\dot{\mathbf{x}}_r(t) - \mathbf{A}\mathbf{V}_r\mathbf{x}_r(t) - \mathbf{B}\,\mathbf{u}(t)\right) = \mathbf{0}, \\ &\mathbf{y}_r(t) = \mathbf{C}\mathbf{V}_r\mathbf{x}_r(t), \end{aligned} \tag{3}$$

("orthogonal residuals"). This leads to $\mathbf{G}_r$ in (2) with

$$\begin{aligned} &\mathbf{E}_r = \mathbf{W}_r^T\mathbf{E}\mathbf{V}_r, \qquad \mathbf{B}_r = \mathbf{W}_r^T\mathbf{B}, \\ &\mathbf{A}_r = \mathbf{W}_r^T\mathbf{A}\mathbf{V}_r, \quad \text{and} \quad \mathbf{C}_r = \mathbf{C}\mathbf{V}_r. \end{aligned} \tag{4}$$

The quality of this reduced model depends solely on the selection of the two subspaces $\mathcal{V}_r$ and $\mathcal{W}_r$, which we choose to enforce interpolation of $\mathbf{G}$ by $\mathbf{G}_r$.

2.1. Interpolatory Petrov–Galerkin projections

The construction of reduced models with interpolatory projections was introduced initially by De Villemagne and Skelton (1987), Yousouff and Skelton (1985) and Yousuff, Wagie, and Skelton (1985) and later put into a robust numerical framework by Grimme (1997). This framework was adapted for MIMO systems of the form (1) by Gallivan, Vandendorpe, and Van Dooren (2005). Beattie and Gugercin (2009b) later extended this to a much larger class of transfer functions, those having a *generalized coprime factorization*, $\mathbf{H}(s) = \mathbf{C}(s)\mathbf{K}(s)^{-1}\mathbf{B}(s)$, where $\mathbf{B}(s)$, $\mathbf{C}(s)$, and $\mathbf{K}(s)$ are given meromorphic matrix-valued functions.

Given a full-order system (1), the *tangential interpolation problem* seeks a reduced system, $\mathbf{G}_r(s)$, that interpolates $\mathbf{G}(s)$ at selected points $\{s_k\}_{k=1}^r \subset \mathbb{C}$ along selected (right) tangent directions $\{\mathbf{b}_k\}_{k=1}^r \subset \mathbb{C}^m$:

$$\mathbf{G}(s_i)\mathbf{b}_i = \mathbf{G}_r(s_i)\mathbf{b}_i, \quad \text{for } i = 1, \ldots, r. \tag{5}$$

Analogous left tangential interpolation conditions may be considered; however (5) will suffice for our purposes. Conditions forcing (5) to be satisfied by a reduced system of the form (4) are provided by Theorem 1 (see Gallivan et al., 2005).

Theorem 1. *Suppose* $\mathbf{G}(s) = \mathbf{C}(s\mathbf{E}-\mathbf{A})^{-1}\mathbf{B}$. *Given a set of distinct interpolation points* $\{s_k\}_{k=1}^r$ *and right tangent directions* $\{\mathbf{b}_k\}_{k=1}^r$, *define* $\mathbf{V}_r \in \mathbb{C}^{n\times r}$ *as*

$$\mathbf{V}_r = \left[(s_1\mathbf{E}-\mathbf{A})^{-1}\mathbf{B}\mathbf{b}_1, \ldots, (s_r\mathbf{E}-\mathbf{A})^{-1}\mathbf{B}\mathbf{b}_r\right]. \tag{6}$$

Then for any $\mathbf{W}_r \in \mathbb{C}^{n\times r}$, *the reduced system* $\mathbf{G}_r(s) = \mathbf{C}_r(s\mathbf{E}_r - \mathbf{A}_r)^{-1}\mathbf{B}_r$ *defined via* (4) *satisfies* (5), *provided that* $s_i\mathbf{E} - \mathbf{A}$ *and* $s_i\mathbf{E}_r - \mathbf{A}_r$ *are all invertible.*

Remark 2. Forcing interpolation of the full transfer function matrix (in *all* input and output directions) will typically inflate the reduced model order by a factor of m (the input dimension). This is neither necessary nor desirable. Effective reduced models, indeed, $\mathcal{H}_2$-*optimal* reduced models, can be generated by forcing interpolation along particular tangent directions.

Remark 3. Theorem 1 can be generalized to include higher-order interpolation (analogous to generalized Hermite interpolation). For example, for a point $\hat{s} \in \mathbb{C}$ and tangent direction $\hat{\mathbf{b}}$, suppose, for $k = 1, \ldots, N$, that

$$\left(\left(\hat{s}\,\mathbf{E} - \mathbf{A}\right)^{-1}\mathbf{E}\right)^{k-1}(\hat{s}\,\mathbf{E} - \mathbf{A})^{-1}\mathbf{B}\hat{\mathbf{b}} \in \text{Range}(\mathbf{V}_r). \tag{7}$$

Then, for any $\mathbf{W}_r \in \mathbb{C}^{n\times r}$, the reduced order system $\mathbf{G}_r(s)$ defined via (2) and (4) satisfies

$$\mathbf{G}^{(\ell)}(\hat{s})\hat{\mathbf{b}} = \mathbf{G}_r^{(\ell)}(\hat{s})\hat{\mathbf{b}}, \quad \text{for } \ell = 0, \ldots, N-1, \tag{8}$$

provided that $\hat{s}\mathbf{E} - \mathbf{A}$ and $\hat{s}\mathbf{E}_r - \mathbf{A}_r$ are invertible where $\mathbf{G}^{(\ell)}(s)$ denotes the ℓth derivative of $\mathbf{G}(s)$. For details see, for example, Antoulas et al. (2010) and Gallivan et al. (2005).

Remark 4. Notice that what guarantees interpolation in Theorem 1 (as well as in Remark 3) is the subspace $\mathcal{V}_r$, not the specific choice of basis in (6). Hence, one may use any matrix $\widehat{\mathbf{V}}_r$ having the same range: $\widehat{\mathbf{V}}_r = \mathbf{V}_r\mathbf{L}$ with invertible $\mathbf{L} \in \mathbb{R}^{r\times r}$ and the interpolation property still holds. This is a simple consequence of the fact that the basis change from $\mathbf{V}_r$ to $\widehat{\mathbf{V}}_r$ amounts to a state-space transformation for the reduced model. When interpolation points are either real or occur in complex conjugate pairs (as always occurs in practice), then the columns of $\mathbf{V}_r$ are also real or occur in conjugate pairs and may be replaced in any case with a *real* basis. We write $\mathbf{V}_r = [\![\mathbf{v}_1, \ldots, \mathbf{v}_r]\!]$ to indicate that a real basis for $\mathbf{V}_r$ is chosen. Notice that this leads to real reduced order quantities in (4).

2.2. Interpolatory optimal $\mathcal{H}_2$ approximation

Let $\mathcal{M}(r)$ denote the set of reduced models as in (2) having state-space dimension r. Given a stable full order system $\mathbf{G}(s) = \mathbf{C}(s\mathbf{E} - \mathbf{A})^{-1}\mathbf{B}$, the optimal-$\mathcal{H}_2$ approximation to $\mathbf{G}(s)$ of order r is a solution to

$$\|\mathbf{G} - \mathbf{G}_r\|_{\mathcal{H}_2} = \min_{\widetilde{\mathbf{G}}_r \in \mathcal{M}(r)} \left\|\mathbf{G} - \widetilde{\mathbf{G}}_r\right\|_{\mathcal{H}_2} \tag{9}$$

where $\|\mathbf{G}\|_{\mathcal{H}_2} := \left(\frac{1}{2\pi}\int_{-\infty}^{\infty}\|\mathbf{G}(\imath\omega)\|_{\mathrm{F}}^2\,d\omega\right)^{1/2}$. The optimization problem (9) is nonconvex, so obtaining a global minimizer is difficult in the best of circumstances. Typically local minimizers are sought instead and as a practical matter, the usual approach is to find reduced models satisfying first-order necessary conditions for $\mathcal{H}_2$-optimality. There are a variety of methods that have been developed to do this. They can be categorized as Lyapunov-based methods such as (Halevi, 1992; Hyland & Bernstein, 1985; Spanos, Milman, & Mingori, 1992; Wilson, 1970; Yan & Lam, 1999; Zigic, Watson, & Beattie, 1993) and interpolation-based methods such as (Beattie & Gugercin, 2007, 2009a; Bunse-Gerstner et al., 2010; Gugercin, 2005; Gugercin et al., 2006, 2008; Kubalinska et al., 2007; Meier & Luenberger, 1967; Van Dooren et al., 2008). Although both frameworks are theoretically equivalent (Gugercin et al., 2008), interpolation-based methods carry some significant computational advantages and that will be our focus.

Interpolation-based $\mathcal{H}_2$-optimality conditions for SISO systems were introduced by Meier and Luenberger (1967). Interpolatory $\mathcal{H}_2$-optimality conditions for MIMO systems have recently been developed by Bunse-Gerstner et al. (2010), Gugercin et al. (2008) and Van Dooren et al. (2008).

Theorem 5. *Suppose that* $\mathbf{G}_r(s) = \sum_{i=1}^{r}\frac{1}{s-\hat{\lambda}_i}\mathbf{c}_i\mathbf{b}_i^T$ *is the best rth order approximation of* $\mathbf{G} = \mathbf{C}(s\mathbf{E} - \mathbf{A})^{-1}\mathbf{B}$ *with respect to the* $\mathcal{H}_2$ *norm and that it has only simple poles. Then for each* $k = 1, 2, \ldots, r$

$$(a)\ \mathbf{G}(-\hat{\lambda}_k)\mathbf{b}_k = \mathbf{G}_r(-\hat{\lambda}_k)\mathbf{b}_k, \tag{10}$$

$$(b)\ \mathbf{c}_k^T\mathbf{G}(-\hat{\lambda}_k) = \mathbf{c}_k^T\mathbf{G}_r(-\hat{\lambda}_k), \quad \textit{and} \tag{11}$$

$$(c)\ \mathbf{c}_k^T\mathbf{G}'(-\hat{\lambda}_k)\mathbf{b}_k = \mathbf{c}_k^T\mathbf{G}_r'(-\hat{\lambda}_k)\mathbf{b}_k. \tag{12}$$

Theorem 5 asserts that any solution to the optimal-$\mathcal{H}_2$ problem (9) must be a bitangential Hermite interpolant to $\mathbf{G}$ at the mirror images of the reduced system poles. This would be a straightforward construction, if the reduced system poles and residues were known *a priori*. However, they are not and the *Iterative Rational Krylov Algorithm (IRKA)* (Gugercin et al., 2008) resolves the problem by iteratively correcting the interpolation points by reflecting the current reduced system poles across the imaginary axis to determine the next set of interpolation points. The next tangent directions are residue directions taken from the current reduced model. Upon convergence, the necessary conditions of Theorem 5 are met. *IRKA* applies interpolatory model reduction at each step using

$$\begin{aligned}\mathbf{V}_r &= [\![(s_1\mathbf{E} - \mathbf{A})^{-1}\mathbf{B}\mathbf{b}_1, \ldots, (s_r\mathbf{E} - \mathbf{A})^{-1}\mathbf{B}\mathbf{b}_r]\!]\\ \mathbf{W}_r &= [\![(s_1\mathbf{E} - \mathbf{A})^{-T}\mathbf{C}^T\mathbf{c}_1, \ldots, (s_r\mathbf{E} - \mathbf{A})^{-T}\mathbf{C}^T\mathbf{c}_r]\!]\end{aligned} \tag{13}$$

where s_i, $\mathbf{b}_i$ and $\mathbf{c}_i$ are, respectively, the interpolation points, and right and left tangent directions at step k of *IRKA*. Note that the Hermite bitangential interpolation conditions (10)–(12) enforce a choice on $\mathbf{W}_r$ as in (13) in contrast to Theorem 1 where $\mathbf{W}_r$ could be chosen arbitrarily. $\mathbf{V}_r$ and $\mathbf{W}_r$ are not constructed explicitly as defined in (13), but rather real matrices with ranges that span the corresponding subspaces are chosen as discussed in Remark 4. For details on *IRKA*, see Gugercin et al. (2008).

3. Linear port-Hamiltonian systems

In the absence of algebraic constraints, linear port-Hamiltonian systems take the following form (Polyuga & van der Schaft, 2011b; The Geoplex Consortium, 2009; van der Schaft, 2000a)

$$\mathbf{G}: \begin{cases}\dot{\mathbf{x}} = (\mathbf{J} - \mathbf{R})\mathbf{Q}\mathbf{x} + \mathbf{B}\,\mathbf{u},\\ \mathbf{y} = \mathbf{B}^T\mathbf{Q}\mathbf{x},\end{cases} \tag{14}$$

where $\mathbf{J} = -\mathbf{J}^T$, $\mathbf{Q} = \mathbf{Q}^T$, and $\mathbf{R} = \mathbf{R}^T \geqslant 0$. $\mathbf{Q}$ is the *energy* matrix; $\mathbf{R}$ is the *dissipation* matrix; $\mathbf{J}$ and $\mathbf{B}$ determine the *interconnection* structure of the system. $H(\mathbf{x}) = \frac{1}{2}\mathbf{x}^T\mathbf{Q}\mathbf{x}$ defines the *total energy* (the *Hamiltonian*). For all cases of interest, $H(\mathbf{x}) \geq 0$. Note that the system (14) has the form (1) with $\mathbf{E} = \mathbf{I}$, $\mathbf{A} = (\mathbf{J} - \mathbf{R})\mathbf{Q}$, and $\mathbf{C} = \mathbf{B}^T\mathbf{Q}$.

The state variables $\mathbf{x} \in \mathbb{R}^n$ are called *energy* variables; the total energy $H(\mathbf{x})$ is expressed as a function of $\mathbf{x}$. $\mathbf{u}, \mathbf{y} \in \mathbb{R}^m$ are called *power* variables; the scalar product $\mathbf{u}^T\mathbf{y}$ is the power supplied to the system. Thus, $\frac{d}{dt}\,\frac{1}{2}\,\mathbf{x}^T\mathbf{Q}\mathbf{x} = \mathbf{u}^T\mathbf{y} - \mathbf{x}^T\mathbf{Q}\mathbf{R}\mathbf{Q}\mathbf{x} \leqslant \mathbf{u}^T\mathbf{y}$, and so port-Hamiltonian systems are *passive* with changes in total system energy bounded by the work done on the system. We assume throughout that $\mathbf{Q}$ is positive definite. In the case of zero dissipation ($\mathbf{R} = \mathbf{0}$), the $\mathbf{G}$ of (14) is both lossless and stable. For positive semidefinite $\mathbf{R}$, $\mathbf{G}$ could be either stable or asymptotically stable in general; and for $\mathbf{R}$ strictly positive definite, the system is asymptotically stable. We assume that $\mathbf{G}$ is merely stable except in Section 5 where we assume asymptotic stability in order to assure a bounded $\mathcal{H}_2$ norm.

Example 1. Consider the ladder network illustrated in Fig. 1, with $C_1, C_2, L_1, L_2, R_1, R_2, R_3$ being, respectively, the capacitances,

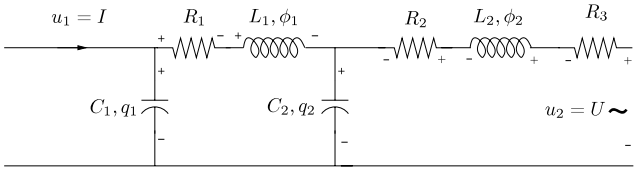

Fig. 1. Ladder network.

inductances, and resistances of idealized linear circuit elements described in the figure. The port-Hamiltonian representation of this physical system has the form (14) with

$$\mathbf{Q} = \mathrm{diag}(C_1^{-1}, L_1^{-1}, C_2^{-1}, L_2^{-1}),$$

$$\mathbf{J} = \mathrm{tridiag}\begin{pmatrix} -1 & -1 & 1 \\ 0 & 0 & 0 & 0 \\ 1 & 1 & -1 \end{pmatrix}, \qquad (15)$$

$$\mathbf{B} = \begin{bmatrix} 1 & 0 \\ 0 & 0 \\ 0 & 0 \\ 0 & 1 \end{bmatrix}$$

and $\mathbf{R} = \mathrm{diag}(0, R_1, 0, R_2 + R_3)$.

The state vector $\mathbf{x}$ is given by $\mathbf{x}^T = [q_1\ \phi_1\ q_2\ \phi_2]$ with q_1, q_2 being the charges on the capacitors C_1, C_2 and ϕ_1, ϕ_2 being the fluxes over the inductors L_1, L_2 correspondingly. The inputs of the system, $\{u_1, u_2\}$ are given by the current I on the left side and the voltage U on the right side of the ladder network. The port-Hamiltonian outputs $\{y_1, y_2\}$ are the voltage over the first capacitor U_{C_1} and the current through the second inductor I_{L_2}.

The system matrices $\mathbf{A}$, $\mathbf{B}$, $\mathbf{C}$, and $\mathbf{E}$ of (1) follow directly from writing the linear input-state differential equation for this system. $\mathbf{Q}$ may be derived from the Hamiltonian $H(\mathbf{x}) = \frac{1}{2}\mathbf{x}^T\mathbf{Q}\mathbf{x}$. Once $\mathbf{A}$ and $\mathbf{Q}$ are known, it is easy to derive the dissipation matrix, $\mathbf{R}$, and the structure matrix, $\mathbf{J}$, corresponding to the Kirchhoff laws, such that $\mathbf{A} = (\mathbf{J} - \mathbf{R})\mathbf{Q}$. The output matrix $\mathbf{C}$ is $\mathbf{C} = \mathbf{B}^T\mathbf{Q}$.

Recall from Polyuga (2010), Polyuga and van der Schaft (2011b) and The Geoplex Consortium (2009) that the port-Hamiltonian system (14) may be represented in *co-energy coordinates* as

$$\dot{\mathbf{e}} = \mathbf{Q}(\mathbf{J} - \mathbf{R})\mathbf{e} + \mathbf{Q}\mathbf{B}\,\mathbf{u}, \qquad \mathbf{y} = \mathbf{B}^T\mathbf{e}. \qquad (16)$$

The state transformation (Polyuga, 2010; The Geoplex Consortium, 2009) between energy coordinates, $\mathbf{x}$, and co-energy coordinates, $\mathbf{e}$, is given by

$$\mathbf{e} = \mathbf{Q}\mathbf{x}. \qquad (17)$$

Example 1 (Continued). The co-energy state vector, $\mathbf{e}$, for the ladder network above is given as $\mathbf{e}^T = \begin{bmatrix} U_{C_1} & I_{L_1} & U_{C_2} & I_{L_2} \end{bmatrix}$ with U_{C_1}, U_{C_2} being the voltages on the capacitors C_1, C_2 and I_{L_1}, I_{L_2} being the currents through the inductors L_1, L_2, respectively.

3.1. Balancing for port-Hamiltonian systems

To make the presentation self-contained, we review a recent structure-preserving, balancing-based model reduction method for port-Hamiltonian systems, the *effort-constraint method* (Polyuga, 2010; Polyuga & van der Schaft, 2008, 2011b, 2012; van der Schaft & Polyuga, 2009), which will be used for comparisons in our numerical examples.

Consider a full order port-Hamiltonian system realized as in (14) with respect to energy coordinates. Consider the associated *balancing transformation*, $\mathbf{T}_b$, defined in the usual way (see Antoulas, 2005 for a complete treatment): $\mathbf{T}_b$ simultaneously diagonalizes the observability Gramian, $\mathbb{G}_o$, and the controllability Gramian, $\mathbb{G}_c$, so that

$$\mathbf{T}_b^{-1}\mathbb{G}_o\mathbf{T}_b^{-T} = \mathbf{T}_b^T\mathbb{G}_c\mathbf{T}_b = \mathrm{diag}(\sigma_1, \sigma_2, \ldots, \sigma_n)$$

where $\sigma_1, \ldots, \sigma_n$ are the Hankel singular values of the system $\mathbf{G}(s)$. This balancing transformation is the same that is used in the context of regular *balanced truncation*.

The state-space transformation associated with balancing (as with any linear coordinate transformation), will preserve port-Hamiltonian structure in (14). Defining *balanced coordinates*, as $\mathbf{x}_b = \mathbf{T}_b\mathbf{x}$, we have

$$\dot{\mathbf{x}}_b = (\mathbf{J}_b - \mathbf{R}_b)\mathbf{Q}_b\mathbf{x}_b + \mathbf{B}_b\mathbf{u}, \qquad \mathbf{y} = (\mathbf{B}_b)^T\mathbf{Q}_b\mathbf{x}_b, \qquad (18)$$

where $\mathbf{B}_b = \mathbf{T}_b\mathbf{B}$, $\mathbf{T}_b\mathbf{R}\mathbf{T}_b^T = \mathbf{R}_b = \mathbf{R}_b^T \geq 0$ is the dissipation matrix, $\mathbf{T}_b\mathbf{J}\mathbf{T}_b^T = \mathbf{J}_b = -\mathbf{J}_b^T$ is the structure matrix and $\mathbf{T}_b^{-T}\mathbf{Q}\mathbf{T}_b^{-1} = \mathbf{Q}_b = \mathbf{Q}_b^T > 0$ is the energy matrix – all represented in balanced coordinates. Split the state vector, $\mathbf{x}_b$, into dominant and codominant components: $\mathbf{x}_b = [\mathbf{x}_{b1}^T\ \mathbf{x}_{b2}^T]^T$ with $\mathbf{x}_{b1} \in \mathbb{R}^r$. Regular balanced truncation directly truncates the codominant state-space components, in effect forcing the system to evolve under the constraint $\mathbf{x}_{b2} = \mathbf{0}$. This destroys port-Hamiltonian structure in the induced reduced system determining the evolution of $\mathbf{x}_{b1}$. In contrast to this, the *effort-constraint method* produces the following reduced order port-Hamiltonian system

$$\begin{aligned} \dot{\mathbf{x}}_{b1} &= (\mathbf{J}_{b11} - \mathbf{R}_{b11})\mathbf{S}_b\mathbf{x}_{b1} + \mathbf{B}_{b1}\mathbf{u}, \\ \mathbf{y}_r &= (\mathbf{B}_{b1})^T\mathbf{S}_b\mathbf{x}_{b1}, \end{aligned} \qquad (19)$$

where $\mathbf{S}_b = \mathbf{Q}_{b11} - \mathbf{Q}_{b12}(\mathbf{Q}_{b22})^{-1}\mathbf{Q}_{b21}$ is the Schur complement of the energy matrix $\mathbf{Q}_b$ in balanced coordinates; the other matrices are of corresponding dimensions. The relationship of the effort-constraint method to the reduction of the underlying (full-order) Dirac structure is discussed in Polyuga (2010), Polyuga and van der Schaft (2012) and van der Schaft and Polyuga (2009). A more direct approach is given in Polyuga and van der Schaft (2011b); another approach using scattering coordinates can be found in Polyuga and van der Schaft (2008).

Remark 6. The effort-constraint method can be formulated with Petrov–Galerkin projections (Polyuga, 2010; Polyuga & van der Schaft, 2012; van der Schaft & Polyuga, 2009). Even though a balancing transformation is used in developing the effort-constraint method as explained above, the method is not equivalent to the usual balanced truncation method. Note that balanced truncation does not preserve port-Hamiltonian structure. For more details, see Polyuga (2010).

4. Interpolatory model reduction of port-Hamiltonian systems

Note that Theorem 1 may be applied to a port-Hamiltonian system with an arbitrary choice of $\mathbf{W}_r$. As a result, $\mathbf{A}_r$ will have the form $\mathbf{W}_r^T(\mathbf{J} - \mathbf{R})\mathbf{Q}\mathbf{V}_r$, which is not evidently in the desired form $(\mathbf{J}_r - \mathbf{R}_r)\mathbf{Q}_r$ with skew-symmetric $\mathbf{J}_r$, symmetric positive semi-definite $\mathbf{R}_r$ and positive definite $\mathbf{Q}_r$. Below, we consider choices for $\mathbf{W}_r$ that preserve port-Hamiltonian structure.

4.1. Interpolatory projection in energy coordinates

We first show how to achieve interpolation and preservation of port-Hamiltonian structure simultaneously in the original energy coordinate representation. The choice of $\mathbf{W}_r$ plays a crucial role.

Theorem 7. *Suppose* $\mathbf{G}(s)$ *is a linear port-Hamiltonian system, as in (14). Let* $\{s_i\}_{i=1}^r \subset \mathbb{C}$ *be a set of* r *distinct interpolation points with corresponding tangent directions* $\{\mathbf{b}_i\}_{i=1}^r \subset \mathbb{C}^m$, *both sets being closed under conjugation. Construct a real matrix* $\mathbf{V}_r$ *from (6) using* $\mathbf{A} = (\mathbf{J}-\mathbf{R})\mathbf{Q}$ *and* $\mathbf{E} = \mathbf{I}$, *so that (cf. Remark 4)*

$$\mathbf{V}_r = [\![(s_1\mathbf{I} - (\mathbf{J}-\mathbf{R})\mathbf{Q})^{-1}\mathbf{B}\mathbf{b}_1, \ldots, (s_r\mathbf{I} - (\mathbf{J}-\mathbf{R})\mathbf{Q})^{-1}\mathbf{B}\mathbf{b}_r]\!].$$

Define $\mathbf{W}_r = \mathbf{Q}\mathbf{V}_r(\mathbf{V}_r^T\mathbf{Q}\mathbf{V}_r)^{-1}$ *and* $\mathbf{J}_r = \mathbf{W}_r^T\mathbf{J}\mathbf{W}_r$, $\mathbf{Q}_r = \mathbf{V}_r^T\mathbf{Q}\mathbf{V}_r$, $\mathbf{R}_r = \mathbf{W}_r^T\mathbf{R}\mathbf{W}_r$, *and* $\mathbf{B}_r = \mathbf{W}_r^T\mathbf{B}$.
The reduced model

$$\mathbf{G}_r : \begin{cases} \dot{\mathbf{x}}_r = (\mathbf{J}_r - \mathbf{R}_r)\mathbf{Q}_r\mathbf{x}_r + \mathbf{B}_r\,\mathbf{u}, \\ \mathbf{y}_r = \mathbf{B}_r^T\mathbf{Q}_r\mathbf{x}_r \end{cases} \tag{20}$$

is port-Hamiltonian, passive, and

$$\mathbf{G}(s_i)\mathbf{b}_i = \mathbf{G}_r(s_i)\mathbf{b}_i, \quad \text{for } i = 1, \ldots, r.$$

That is, $\mathbf{G}_r(s)$ *interpolates* $\mathbf{G}(s)$ *at* $\{s_i\}_{i=1}^r$ *along the tangent directions* $\{\mathbf{b}_i\}_{i=1}^r$.

Proof. If there are complex vectors among the primitive basis vectors given, they must occur in conjugate pairs and so, in light of Remark 4, there will be a real choice of basis $\mathbf{V}_r \in \mathbb{R}^{n\times r}$. The reduced system (20) is then also real, retains port-Hamiltonian structure with a positive definite $\mathbf{Q}_r$, and so must be passive. To see that $\mathbf{G}_r(s)$ interpolates $\mathbf{G}(s)$ note, as before, that the port-Hamiltonian system (14) has the standard form (1) with $\mathbf{E} = \mathbf{I}$, $\mathbf{A} = (\mathbf{J}-\mathbf{R})\mathbf{Q}$, and $\mathbf{C} = \mathbf{B}^T\mathbf{Q}$. An interpolatory reduced model may be defined using (2) and (4). We then have $\mathbf{E}_r = \mathbf{W}_r^T\mathbf{V}_r = \mathbf{I}_r$ and $\mathbf{A}_r = \mathbf{W}_r^T\mathbf{A}\mathbf{V}_r = \mathbf{W}_r^T(\mathbf{J}-\mathbf{R})\mathbf{Q}\mathbf{V}_r$. From Theorem 1, this model interpolates $\mathbf{G}(s)$ at $\{s_i\}_{i=1}^r$ along the tangent directions $\{\mathbf{b}_i\}_{i=1}^r$ as required but it is not obvious that this is the same reduced system $\mathbf{G}_r(s)$ that we have defined above.

Note that $\mathbf{W}_r\mathbf{V}_r^T$ is a (skew) projection onto Range$(\mathbf{Q}\mathbf{V}_r)$ and so $\mathbf{Q}\mathbf{V}_r = \mathbf{W}_r\mathbf{V}_r^T\mathbf{Q}\mathbf{V}_r$. Thus, we have

$$\begin{aligned}\mathbf{A}_r &= \mathbf{W}_r^T(\mathbf{J}-\mathbf{R})\mathbf{Q}\mathbf{V}_r = \mathbf{W}_r^T(\mathbf{J}-\mathbf{R})\mathbf{W}_r\mathbf{V}_r^T\mathbf{Q}\mathbf{V}_r \\ &= (\mathbf{W}_r^T\mathbf{J}\mathbf{W}_r - \mathbf{W}_r^T\mathbf{R}\mathbf{W}_r)\mathbf{V}_r^T\mathbf{Q}\mathbf{V}_r = (\mathbf{J}_r - \mathbf{R}_r)\mathbf{Q}_r\end{aligned}$$

and $\mathbf{C}_r = \mathbf{C}\mathbf{V}_r = \mathbf{B}^T\mathbf{Q}\mathbf{V}_r = \mathbf{B}^T\mathbf{W}_r\mathbf{V}_r^T\mathbf{Q}\mathbf{V}_r = \mathbf{B}_r^T\mathbf{Q}_r$. Thus, the reduced port-Hamiltonian system, $\mathbf{G}_r(s)$, interpolates $\mathbf{G}(s)$ at $\{s_i\}_{i=1}^r$ along $\{\mathbf{b}_i\}_{i=1}^r$ as required. □

Remark 8. Following on Remark 3, Theorem 7 can be generalized to include generalized Hermite derivative interpolation by augmenting $\mathbf{V}_r$ appropriately so that (7) holds. The construction of Theorem 7 proceeds unchanged and the resulting reduced model retains port-Hamiltonian structure (hence is both stable and passive) and will interpolate derivatives of $\mathbf{G}(s)$ as in (8).

4.2. The influence of state-space transformations

Let $\mathbf{T} \in \mathbb{R}^{n\times n}$ be an arbitrary invertible matrix representing a state-space transformation $\tilde{\mathbf{x}} = \mathbf{T}\mathbf{x}$. As one may recall from the discussion of Section 3.1, port-Hamiltonian structure will be maintained under state-space transformations:

$$\begin{aligned}&\dot{\mathbf{x}} = (\mathbf{J}-\mathbf{R})\mathbf{Q}\mathbf{x} + \mathbf{B}\,\mathbf{u}, \\ &\mathbf{y} = \mathbf{B}^T\mathbf{Q}\mathbf{x}.\end{aligned} \iff \begin{aligned}&\dot{\tilde{\mathbf{x}}} = (\widetilde{\mathbf{J}}-\widetilde{\mathbf{R}})\widetilde{\mathbf{Q}}\tilde{\mathbf{x}} + \widetilde{\mathbf{B}}\,\mathbf{u}, \\ &\mathbf{y} = \widetilde{\mathbf{B}}^T\widetilde{\mathbf{Q}}\tilde{\mathbf{x}}\end{aligned}$$

with transformed quantities $\widetilde{\mathbf{J}} = \mathbf{T}\mathbf{J}\mathbf{T}^T$, $\widetilde{\mathbf{R}} = \mathbf{T}\mathbf{R}\mathbf{T}^T$, $\widetilde{\mathbf{Q}} = \mathbf{T}^{-T}\mathbf{Q}\mathbf{T}^{-1}$, and $\widetilde{\mathbf{B}} = \mathbf{T}\mathbf{B}$.

Theorem 9. *Suppose* $\mathbf{G}(s)$ *is a port-Hamiltonian system as in (14), with two port-Hamiltonian realizations connected via a state-space transformation,* $\mathbf{T}$, *as above. Given a set of* r *distinct interpolation points* $\{s_i\}_{i=1}^r \subset \mathbb{C}$ *with tangent directions* $\{\mathbf{b}_i\}_{i=1}^r \subset \mathbb{C}^m$ *(closed under conjugation), then the interpolatory reduced port-Hamiltonian models produced from either realization via Theorem 7 will be identical to one another.*

Proof. Define real interpolatory basis matrices for each realization as

$$\mathbf{V}_r = [\![(s_1\mathbf{I} - (\mathbf{J}-\mathbf{R})\mathbf{Q})^{-1}\mathbf{B}\mathbf{b}_1, \ldots, (s_r\mathbf{I} - (\mathbf{J}-\mathbf{R})\mathbf{Q})^{-1}\mathbf{B}\mathbf{b}_r]\!]$$

and

$$\widetilde{\mathbf{V}}_r = [\![(s_1\mathbf{I} - (\widetilde{\mathbf{J}}-\widetilde{\mathbf{R}})\widetilde{\mathbf{Q}})^{-1}\widetilde{\mathbf{B}}\mathbf{b}_1, \ldots, (s_r\mathbf{I} - (\widetilde{\mathbf{J}}-\widetilde{\mathbf{R}})\widetilde{\mathbf{Q}})^{-1}\widetilde{\mathbf{B}}\mathbf{b}_r]\!].$$

Without loss of generality, we may assume that $\widetilde{\mathbf{V}}_r = \mathbf{T}\mathbf{V}_r$ since any change of basis that makes $\mathbf{V}_r$ real will make $\widetilde{\mathbf{V}}_r$ real as well, starting from each of the primitive (complex) bases given. Then we define, following the construction of Theorem 7, $\mathbf{W}_r = \mathbf{Q}\mathbf{V}_r$ and $\widetilde{\mathbf{W}}_r = \widetilde{\mathbf{Q}}\widetilde{\mathbf{V}}_r$. Observe that $\widetilde{\mathbf{W}}_r = \mathbf{T}^{-T}\mathbf{W}_r$. So, $\mathbf{J}_r = \mathbf{W}_r^T\mathbf{J}\mathbf{W}_r = \widetilde{\mathbf{W}}_r^T\widetilde{\mathbf{J}}\widetilde{\mathbf{W}}_r = \widetilde{\mathbf{J}}_r$, $\mathbf{Q}_r = \mathbf{V}_r^T\mathbf{Q}\mathbf{V}_r = \widetilde{\mathbf{V}}_r^T\widetilde{\mathbf{Q}}\widetilde{\mathbf{V}}_r = \widetilde{\mathbf{Q}}_r$, $\mathbf{R}_r = \mathbf{W}_r^T\mathbf{R}\mathbf{W}_r = \widetilde{\mathbf{W}}_r^T\widetilde{\mathbf{R}}\widetilde{\mathbf{W}}_r = \widetilde{\mathbf{R}}_r$, and $\mathbf{B}_r = \mathbf{W}_r^T\mathbf{B} = \widetilde{\mathbf{W}}_r^T\widetilde{\mathbf{B}} = \widetilde{\mathbf{B}}_r$. □

Remark 10. One may conclude from Theorem 9 that prior to calculating an interpolatory reduced model, there may be little advantage in first applying a state-space transformation, e.g., applying a balancing transformation, $\mathbf{T}_b$, as described in Section 3.1 or transforming to co-energy coordinates with $\mathbf{T} = \mathbf{Q}$ as in (17). Indeed, choosing a realization that exhibits advantageous sparsity patterns that facilitate the linear system solves necessary to produce $\mathbf{V}_r$ will likely be the most effective choice. If we choose $\mathbf{T}$ to satisfy $\mathbf{T}^T\mathbf{T} = \mathbf{Q}$ (for example, if $\mathbf{T}$ is a Cholesky factor for $\mathbf{Q}$) then, with respect to the new $\tilde{\mathbf{x}}$-coordinates (called "scaled energy coordinates"), we find that $\widetilde{\mathbf{Q}} = \mathbf{I}$ and so $\widetilde{\mathbf{W}}_r = \widetilde{\mathbf{V}}_r$. Notice that in this case, scaled energy coordinates and scaled co-energy coordinates become identical. Notwithstanding these simplifications, unless the original $\mathbf{Q}$ is diagonal (so that the transformation to scaled energy coordinates preserves sparsity), there appears to be little justification for global coordinate transformations preceding the construction of an interpolatory reduced model.

5. $\mathcal{H}_2$-reduction of port-Hamiltonian systems

Inspired by the optimal $\mathcal{H}_2$ model reduction method described in Section 2.2, we propose here an algorithm similar to *IRKA* of Gugercin et al. (2008) that is consistently observed to produce high quality port-Hamiltonian reduced models of port-Hamiltonian systems.

Algorithm 1. ***(IRKA-PH)*** **IRKA for MIMO port-Hamiltonian systems.**

Let $\mathbf{G}(s) = \mathbf{B}^T\mathbf{Q}(s\mathbf{I} - (\mathbf{J}-\mathbf{R})\mathbf{Q})^{-1}\mathbf{B}$ as in (14).

(1) Choose initial interpolation points $\{s_1, \ldots, s_r\}$ and tangent directions $\{\mathbf{b}_1, \ldots, \mathbf{b}_r\}$. Both sets closed under conjugation.
(2) Construct a (real) matrix (cf. Remark 4):
$\mathbf{V}_r = [\![(s_1\mathbf{I} - (\mathbf{J}-\mathbf{R})\mathbf{Q})^{-1}\mathbf{B}\mathbf{b}_1, \ldots, (s_r\mathbf{I} - (\mathbf{J}-\mathbf{R})\mathbf{Q})^{-1}\mathbf{B}\mathbf{b}_r]\!]$.
(3) Calculate $\mathbf{W}_r = \mathbf{Q}\mathbf{V}_r(\mathbf{V}_r^T\mathbf{Q}\mathbf{V}_r)^{-1}$
(4) repeat until convergence
  (a) Calculate $\mathbf{J}_r = \mathbf{W}_r^T\mathbf{J}\mathbf{W}_r$, $\mathbf{R}_r = \mathbf{W}_r^T\mathbf{R}\mathbf{W}_r$, $\mathbf{Q}_r = \mathbf{V}_r^T\mathbf{Q}\mathbf{V}_r$ and $\mathbf{B}_r = \mathbf{W}_r^T\mathbf{B}$.
  (b) For $\mathbf{A}_r = (\mathbf{J}_r - \mathbf{R}_r)\mathbf{Q}_r$, compute $\mathbf{A}_r\mathbf{x}_i = \lambda_i\mathbf{x}_i$, $\mathbf{y}_i^*\mathbf{A}_r = \lambda_i\mathbf{y}_i^*$ with $\mathbf{y}_i^*\mathbf{x}_j = \delta_{ij}$ for left and right eigenvectors $\mathbf{y}_i^*$ and $\mathbf{x}_i$ associated with λ_i.
  (c) $s_i \leftarrow -\lambda_i$ and $\mathbf{b}_i^T \leftarrow \mathbf{y}_i^*\mathbf{B}_r$ for $i = 1, \ldots, r$.
  (d) Compute a (real) matrix (cf. Remark 4):
  $\mathbf{V}_r = [\![(s_1\mathbf{I} - (\mathbf{J}-\mathbf{R})\mathbf{Q})^{-1}\mathbf{B}\mathbf{b}_1, \ldots, (s_r\mathbf{I} - (\mathbf{J}-\mathbf{R})\mathbf{Q})^{-1}\mathbf{B}\mathbf{b}_r]\!]$.
  (e) Calculate $\mathbf{W}_r = \mathbf{Q}\mathbf{V}_r(\mathbf{V}_r^T\mathbf{Q}\mathbf{V}_r)^{-1}$
(5) The final reduced model is given by
$\mathbf{J}_r = \mathbf{W}_r^T\mathbf{J}\mathbf{W}_r$, $\mathbf{R}_r = \mathbf{W}_r^T\mathbf{R}\mathbf{W}_r$, $\mathbf{B}_r = \mathbf{W}_r^T\mathbf{B}$,
$\mathbf{Q}_r = \mathbf{V}_r^T\mathbf{Q}\mathbf{V}_r$, and $\mathbf{C}_r = \mathbf{B}_r^T\mathbf{Q}_r$.

Algorithm 1 is an adaptation of *IRKA* (Gugercin et al., 2008). It enforces (10), one of the first-order $\mathcal{H}_2$-optimality conditions, at every step. It is generally not possible to satisfy all optimality conditions (10)–(12) while still retaining port-Hamiltonian structure, so the remaining conditions (11)–(12) are abandoned in order to preserve port-Hamiltonian structure. This trade-off may also be viewed with regards to the choice for $\mathbf{W}_r$: choosing $\mathbf{V}_r$ as in (13) forces (10); additionally choosing $\mathbf{W}_r$ as in (13) would force (11)–(12); but instead, we choose $\mathbf{W}_r$ as in Theorem 7 in order to preserve port-Hamiltonian structure. (See, however, Remark 13).

The convergence behavior of *IRKA-PH* appears similar to that of *IRKA*, which has been studied in detail in Gugercin et al. (2008); see also Antoulas et al. (2010). Effective initialization strategies have been proposed in Gugercin et al. (2008), although random initialization often performs very well. We illustrate the robustness of *IRKA-PH* with regard to initialization in Section 6.

Theorem 11. *Let* $\mathbf{G}(s) = \mathbf{B}^T\mathbf{Q}(s\mathbf{I}-(\mathbf{J}-\mathbf{R})\mathbf{Q})^{-1}\mathbf{B}$ *be an asymptotically stable, port-Hamiltonian system as in (14). Suppose IRKA-PH as described in Algorithm* 1 *converges to a reduced model*

$$\mathbf{G}_r(s) = \sum_{i=1}^{r} \frac{1}{s-\lambda_i}\mathbf{c}_i\mathbf{b}_i^T, \tag{21}$$

with r distinct poles, $\{\lambda_1, \ldots, \lambda_r\}$. *Then* $\mathbf{G}_r(s)$ *is port-Hamiltonian, asymptotically stable, and passive. Moreover,* $\mathbf{G}_r(s)$ *satisfies the necessary condition (10), for* $\mathcal{H}_2$ *optimality:* $\mathbf{G}_r(s)$ *interpolates* $\mathbf{G}(s)$ *at* $-\lambda_i$ *along the tangent directions* $\mathbf{b}_i$ *for* $i = 1, \ldots, r$.

Notice that $\mathbf{G}(s)$ must be asymptotically stable in any case for the $\mathcal{H}_2$ norm to be well defined.

Proof. Port-Hamiltonian structure, and thus passivity, are direct consequences of the construction of $\mathbf{G}_r$ in Theorem 7. The $\mathcal{H}_2$-optimality condition (10) results from the assignment of interpolation points, s_i, and tangent directions, $\mathbf{b}_i$, in Step 4-c throughout the iteration. Upon convergence, $s_i = -\lambda_i$ and $\mathbf{b}_i$ is the right residue of $\mathbf{G}_r$ corresponding to the pole λ_i.

To prove asymptotic stability we proceed as follows. Referring to Theorem 9, we can assume that $\mathbf{Q} = \mathbf{I}$ without loss of generality. Since any choice of a real matrix with the same range as $\mathbf{V}_r$ in Steps 2 and 4-d of Algorithm 1 may be made, choose $\mathbf{V}_r$ to be orthogonal, i.e., $\mathbf{V}_r^T\mathbf{V}_r = \mathbf{I}_r$. Then $\mathbf{W}_r = \mathbf{V}_r$ and the associated reduced quantities are given by one-sided projection: $\mathbf{A}_r = \mathbf{V}_r^T\mathbf{A}\mathbf{V}_r$ and $\mathbf{B}_r = \mathbf{C}_r^T = \mathbf{V}_r^T\mathbf{B}$. Let $\mathbf{A}_r = \mathbf{X}_r\mathbf{\Lambda}\mathbf{X}_r^{-1}$ be the eigenvalue decomposition of $\mathbf{A}_r$ with $\mathbf{\Lambda} = \mathrm{diag}(\lambda_1, \ldots, \lambda_r)$. The tangent directions $\mathbf{b}_i$ satisfy $[\mathbf{b}_1, \ldots, \mathbf{b}_r] = \mathbf{B}^T\mathbf{V}_r\mathbf{X}_r^{-T}$. Define $\hat{\mathbf{v}}_i = (-\lambda_i\mathbf{I} - \mathbf{A})^{-1}\mathbf{B}\mathbf{b}_i$ for $i = 1, \ldots, r$ and $\widehat{\mathbf{V}}_r = \left[\hat{v}_1, \hat{v}_2, \ldots, \hat{v}_r\right]$. From the definition of $\hat{\mathbf{v}}_i$, we have

$$\mathbf{A}\widehat{\mathbf{V}}_r + \widehat{\mathbf{V}}_r\mathbf{\Lambda}^T + \mathbf{B}\mathbf{B}^T\mathbf{V}_r\mathbf{X}_r^{-T} = \mathbf{0}. \tag{22}$$

Since the projecting subspace, $\mathcal{V}_r$, which determines $\mathbf{G}_r$ has converged, $\mathrm{Range}(\widehat{\mathbf{V}}_r) = \mathrm{Range}(\mathbf{V}_r)$ and there is a nonsingular matrix, $\mathbf{M}_r$, such that $\widehat{\mathbf{V}}_r = \mathbf{V}_r\mathbf{M}_r$. Define $\mathbf{N}_r = \mathbf{M}_r\mathbf{X}_r^T$ and rearrange (22) to get

$$\mathbf{A}\mathbf{V}_r\mathbf{N}_r + \mathbf{V}_r\mathbf{N}_r\mathbf{A}_r^T + \mathbf{B}\mathbf{B}_r^T = \mathbf{0}. \tag{23}$$

Premultiplying by $\mathbf{V}_r^T$ yields

$$\mathbf{A}_r\mathbf{N}_r + \mathbf{N}_r\mathbf{A}_r^T + \mathbf{B}_r\mathbf{B}_r^T = \mathbf{0}. \tag{24}$$

Since $\mathbf{G}_r(s)$ is passive, we know that $\mathbf{A}_r$ has no eigenvalues in the open right-half plane. To prove asymptotic stability of $\mathbf{G}_r(s)$, we need to show further that $\mathbf{A}_r$ has no eigenvalues on the imaginary axis. Assume the contrary, so that for some nontrivial vector, $\mathbf{z}_r$, and real ω, $\mathbf{z}_r^*\mathbf{A}_r = \imath\omega\mathbf{z}_r^*$ and $\mathbf{A}_r^T\mathbf{z}_r = -\imath\omega\,\mathbf{z}_r$. Multiply (24) by $\mathbf{z}_r^*$ from the left and by $\mathbf{z}_r$ from the right to find: $\mathbf{B}_r^T\mathbf{z}_r = 0$.

Now, multiplying (23) from the right by $\mathbf{z}_r$ leads to $\mathbf{A}\,(\mathbf{V}_r\mathbf{N}_r\mathbf{z}_r) = \imath\omega\ (\mathbf{V}_r\mathbf{N}_r\mathbf{z}_r)$, which contradicts the asymptotic stability of $\mathbf{G}(s)$. Therefore, the poles of $\mathbf{G}_r(s)$ must lie in the open left half-plane and $\mathbf{G}_r(s)$ is asymptotically stable. □

Remark 12. Let $\mathcal{PH}(r)$ denote the set of port-Hamiltonian systems with state-space dimension r as in (20) and consider the problem:

$$\|\mathbf{G} - \mathbf{G}_r\|_{\mathcal{H}_2} = \min_{\widetilde{\mathbf{G}}_r \in \mathcal{PH}(r)} \left\|\mathbf{G} - \widetilde{\mathbf{G}}_r\right\|_{\mathcal{H}_2} \tag{25}$$

where $\mathbf{G}$ and $\mathbf{G}_r$ are both port-Hamiltonian. This is the problem that we would prefer to solve and it is a topic of current research. Note that although *IRKA-PH* generates a reduced-order port-Hamiltonian model, $\mathbf{G}_r$, satisfying a first-order necessary condition for $\mathcal{H}_2$ optimality, this condition is not a necessary condition for $\mathbf{G}_r$ to solve (25), that is, for $\mathbf{G}_r$ to be the *optimal* reduced-order port-Hamiltonian system approximation to the port-Hamiltonian system $\mathbf{G}$. Nonetheless, we find that reduced-order models produced by *IRKA-PH* have much superior $\mathcal{H}_2$ performance compared to other approaches. This is illustrated in Section 6.

Remark 13. *IRKA-PH*, as described in Algorithm 1, produces a reduced order port-Hamiltonian model $\mathbf{G}_r$, which satisfies the first-order necessary condition of $\mathcal{H}_2$-optimality (10). The remaining two conditions for $\mathcal{H}_2$-optimality, (11) and (12), will be satisfied if in addition:

$$\begin{aligned}&\mathrm{Range}[(\lambda_1\mathbf{I} + (\mathbf{J}-\mathbf{R})\mathbf{Q})^{-1}\mathbf{B}\mathbf{b}_1, \ldots, (\lambda_r\mathbf{I} + (\mathbf{J}-\mathbf{R})\mathbf{Q})^{-1}\mathbf{B}\mathbf{b}_r]\\ &\quad = \mathrm{Range}[(\lambda_1\mathbf{I} + (\mathbf{J}-\mathbf{R})^T\mathbf{Q})^{-1}\mathbf{B}\mathbf{c}_1, \ldots, (\lambda_r\mathbf{I}\\ &\qquad + (\mathbf{J}-\mathbf{R})^T\mathbf{Q})^{-1}\mathbf{B}\mathbf{c}_r],\end{aligned} \tag{26}$$

where λ_i are reduced system poles and $\mathbf{b}_i$, $\mathbf{c}_i$ are the corresponding (vector) residues in the expansion (21) for $i = 1, \ldots, r$. The condition (26) allows retention of port-Hamiltonian structure while enforcing the $\mathcal{H}_2$-optimal bitangential interpolation conditions (10)–(12). Typically (26) will not hold; however the special case when $\mathbf{J} = \mathbf{0}$ will lead to (26) with $\mathbf{b}_i = \mathbf{c}_i$ implying satisfaction of $\mathcal{H}_2$ optimality conditions for the reduced system.

6. Numerical examples

We illustrate the preceding theoretical discussion on three port-Hamiltonian systems. The first two are of modest dimension allowing us to compute $\mathcal{H}_2$ and $\mathcal{H}_\infty$ system errors explicitly for full comparisons. Then, to illustrate that our proposed method can be easily applied in large-scale settings as intended, we consider a large-scale model in the third example.

6.1. MIMO mass–spring–damper system

The full model we consider is a mass–spring–damper system shown in Fig. 2, with masses m_i, spring constants k_i and damping constants $c_i \geq 0$, $i = 1, \ldots, n/2$. q_i is the displacement of the mass m_i. The inputs u_1, u_2 are the external forces applied to the first two masses m_1, m_2. The port-Hamiltonian outputs y_1, y_2 are the velocities of the masses m_1, m_2. The state variables are as follows: x_1 is the displacement q_1 of the first mass m_1, x_2 is the momentum p_1 of the first mass m_1, x_3 is the displacement q_2 of the second mass m_2, x_4 is the momentum p_2 of the second mass m_2, etc.

A minimal realization of this port-Hamiltonian system corresponding to three masses, three springs and three dampers, i.e. $n = 6$, is $\mathbf{G}(s) = \mathbf{B}^T\mathbf{Q}(\mathbf{I} - (\mathbf{J}-\mathbf{R}))^{-1}\mathbf{B}$ where $\mathbf{B} \in \mathbb{R}^{6\times 2}$, $\mathbf{R} \in \mathbb{R}^{6\times 6}$ are

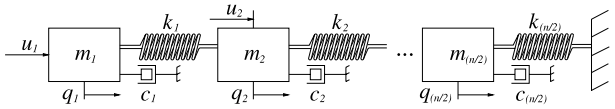

Fig. 2. Mass–spring–damper system.

zero matrices except the entries $\mathbf{B}(2,1) = \mathbf{B}(4,2) = 1$; $\mathbf{J}(1,2) = \mathbf{J}(3,4) = \mathbf{J}(5,6) = 1, \mathbf{J}(2,1) = \mathbf{J}(4,3) = \mathbf{J}(6,5) = -1$; and $\mathbf{R}(2,2) = c_1, \mathbf{R}(4,4) = c_2$, and $\mathbf{R}(6,6) = c_3$. Also,

$$\mathbf{Q} = \begin{bmatrix} k_1 & 0 & -k_1 & 0 & 0 & 0 \\ 0 & \frac{1}{m_1} & 0 & 0 & 0 & 0 \\ -k_1 & 0 & k_1+k_2 & 0 & -k_2 & 0 \\ 0 & 0 & 0 & \frac{1}{m_2} & 0 & 0 \\ 0 & 0 & -k_2 & 0 & k_2+k_3 & 0 \\ 0 & 0 & 0 & 0 & 0 & \frac{1}{m_3} \end{bmatrix}$$

and $\mathbf{A} = (\mathbf{J} - \mathbf{R})\mathbf{Q}$.

Each additional mass–spring–damper cell increases the dimension of the system by two. This will lead to a zero entry in the $(n-1, n-1)$ position and an entry of $-c_{n/2}/m_{n/2}$ in the (n, n) position. The superdiagonal of $\mathbf{A}$ will have $k_{n/2-1}$ in the $(n-2, n-1)$ position and $1/m_{n/2}$ in the $(n-1, n)$ position. The subdiagonal of $\mathbf{A}$ will have 0 in the $(n-1, n-2)$ position and $-k_{n/2-1} - k_{n/2}$ in the $(n, n-1)$ position. Additionally $\mathbf{A}$ will have $k_{n/2-1}$ in the $(n, n-3)$ position.

We used a 100-dimensional mass–spring–damper system with $m_i = 4$, $k_i = 4$, and $c_i = 1$. We consider three methods: (1) our proposed method in Algorithm 1 denoted *IRKA-PH*; (2) the effort-constraint method (19) of Polyuga (2010), Polyuga and van der Schaft (2008, 2011b, 2012) and van der Schaft and Polyuga (2009) denoted *EffBal*, and (3) one step of interpolatory model reduction without the $\mathcal{H}_2$ iteration, denoted 1*stepIntrp*. *IRKA-PH* and 1*stepIntrp* are connected in the following way: We choose a set of interpolation points and tangential directions; then using the interpolatory projection in Theorem 7, a reduced model is produced which we assign to 1*stepIntrp*. The same interpolation points and directions are used to initialize *IRKA-PH*. This allows us to evaluate how well *IRKA-PH* corrects interpolation points and directions, in terms of $\mathcal{H}_2$ and $\mathcal{H}_\infty$ behavior.

Using each of the three methods, we reduce the order to $r = 2, 4, \ldots, 20$ (increments of two). For *IRKA-PH*, initial interpolation points are chosen as logarithmically spaced points between 10^{-3} and 10^{-1}; and the corresponding directions are the dominant right singular vectors of the 2×2 transfer function matrix at each interpolation point. These same points and directions are also used for 1*stepIntrp*. The resulting relative $\mathcal{H}_2$ and $\mathcal{H}_\infty$ error norms for each order r are illustrated in Fig. 3. Several observations are immediate. First of all, with respect to both the $\mathcal{H}_2$ and $\mathcal{H}_\infty$ norms, *IRKA-PH* significantly outperforms the other methods. For 1*stepIntrp*, the performance hardly improves as r increases unlike *IRKA-PH* for which both the $\mathcal{H}_2$ and $\mathcal{H}_\infty$ errors decay consistently. The initial interpolation point and direction selection does not yield a satisfactory interpolatory reduced-order model; however, instead of searching for better interpolation data in an *ad hoc* way, our proposed method automatically corrects interpolation data throughout the iteration and yields significantly smaller error. To see this effect more clearly, we plot in Fig. 4 the initial interpolation point selection, denoted by $s^{\{0\}}$, and the final/converged interpolation points, denoted by $s^{\{\text{final}\}}$, together with the mirror images of the original system poles, denoted by $-\lambda_i$. Starting with logarithmically placed points, *IRKA-PH* iteratively corrects the points so that upon convergence they

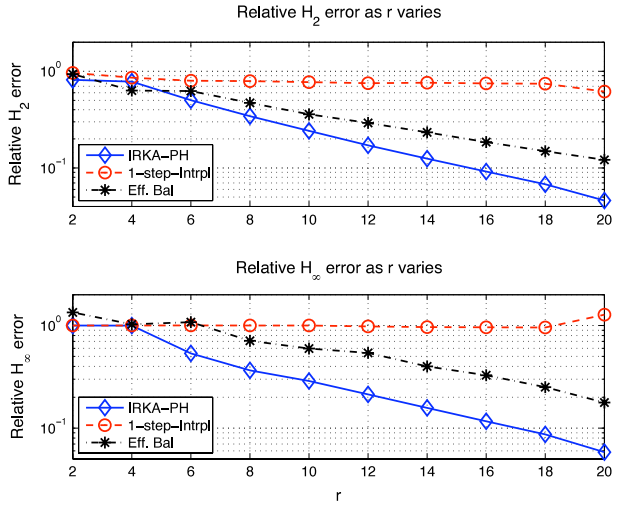

Fig. 3. Relative $\mathcal{H}_2$ and $\mathcal{H}_\infty$ norms for mass–spring–damper system.

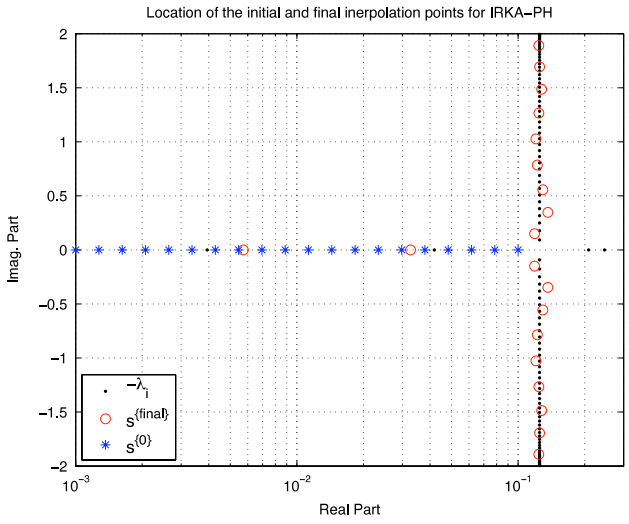

Fig. 4. Initial and converged interpolation points for mass–spring–damper system for $r = 20$.

automatically align themselves in a way that balances the original system poles across the imaginary axis. This is similar to what one finds in the analysis of iterative methods where Ritz values provide effective aggregate information about the spectrum, better than is possible even with a subset of exact eigenvalues. Note that full-order poles are computed here only to obtain this figure and are not needed by *IRKA-PH*.

The second observation concerning Fig. 3 is that *IRKA-PH* achieves smaller error with less computational effort than *EffBal*; the main cost is sparse linear solves. No dense matrix operations are needed, unlike the balancing-based approaches where Lyapunov equations need to be solved. Even though our proposed method is $\mathcal{H}_2$-based, it produces satisfactory $\mathcal{H}_\infty$ performance as well. This is consistent with experiences with *IRKA* (Gugercin et al., 2008), which usually exhibits good $\mathcal{H}_\infty$ performance.

Consider, in Fig. 5, how the $\mathcal{H}_2$ and $\mathcal{H}_\infty$ errors evolve during *IRKA-PH* for $r = 20$, the largest reduction order. The figure reveals convergence within seven or eight steps. The large initial relative errors are reduced drastically already after two steps of the iteration, illustrating the effectiveness of *IRKA-PH*.

Next, we investigate the effect of different initializations on the performance of *IRKA-PH*. For brevity, we only illustrate the $r = 20$ case. We make 5 different initializations and denote by $s_0^{\{j\}}$ the set

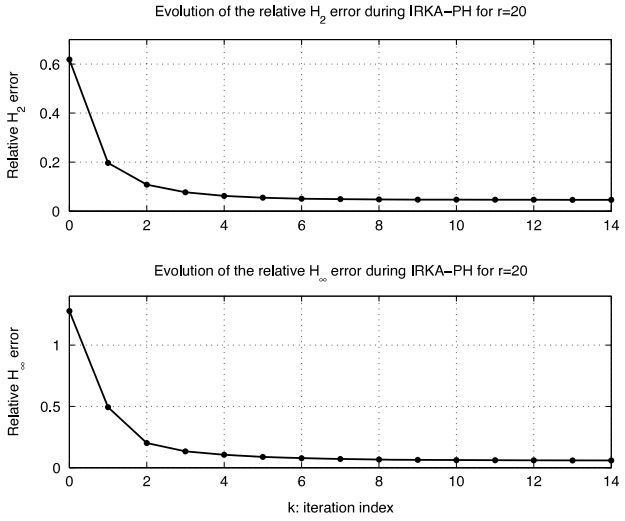

Fig. 5. Relative $\mathcal{H}_2$ and $\mathcal{H}_\infty$ norms for mass–spring–damper system.

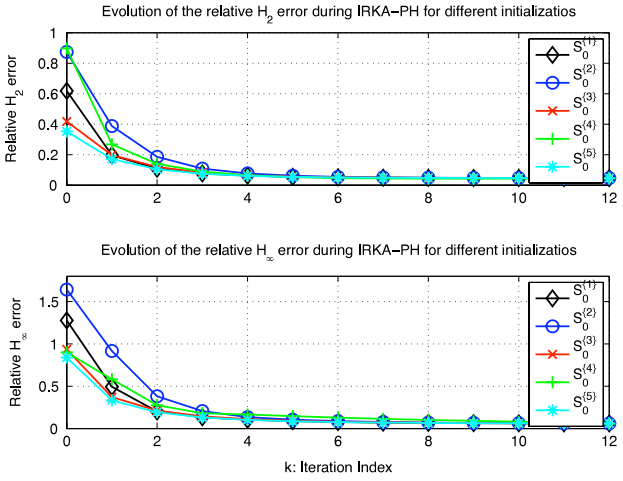

Fig. 6. Relative $\mathcal{H}_2$ and $\mathcal{H}_\infty$ norms for different initializations for mass–spring–damper system for $r = 20$.

of initial interpolation points corresponding to the jth selection. $\mathcal{S}_0^{\{1\}}$ will be the same as what was used earlier, i.e., 20 points logarithmically spaced between 10^{-3} and 10^{-1}. For $\mathcal{S}_0^{\{2\}}$, we choose 20 points logarithmically spaced between -10^{-5} and -10^{-2}. Note that this is a poor selection since these initial interpolation points lie in the left-half plane in proximity of the poles. We consciously make this (bad) choice to see the effect on convergence. For $\mathcal{S}_0^{\{3\}}$, we choose complex points in the right half-plane with real parts that are logarithmically spaced between 10^{-6} and 1 and imaginary parts that are logarithmically spaced between 10^{-3} and 10^{-1}, and such that the set is closed under conjugation. These points are arbitrarily selected and are unrelated to the spectrum of $\mathbf{A}$. For $\mathcal{S}_0^{\{4\}}$, we make the situation even worse than for $\mathcal{S}_0^{\{2\}}$. We choose 20 poles of the original system, $\mathbf{G}(s)$, and perturb them by 0.1% to obtain our starting points. This is a very bad selection in two respects: (1) the interpolation points lie in the left-half plane; and (2) they are extremely close to system poles and make the linear system $(s_i\mathbf{E} - \mathbf{A})\mathbf{v}_i = \mathbf{B}\mathbf{b}_i$ very poorly conditioned. Finally, for $\mathcal{S}_0^{\{5\}}$ we choose, once again, 20 original system poles, but this time reflect them across the imaginary axis to obtain initialization points. Associated directions are taken as before to be dominant right singular vectors of the transfer function evaluated at each interpolation point.

Fig. 6 shows the evolution of relative $\mathcal{H}_2$ and $\mathcal{H}_\infty$ errors during *IRKA-PH* for these 5 different selections. In all cases, *IRKA-PH* converges to the same reduced-model in almost the same number of steps. As expected, $\mathcal{S}_0^{\{2\}}$ and $\mathcal{S}_0^{\{4\}}$ are the worst initializations, starting with relative errors bigger than 1 in the $\mathcal{H}_\infty$ norm. However, the algorithm successfully corrects these points and drives them towards high-fidelity interpolation points and tangent directions. Even though $\mathcal{S}_0^{\{5\}}$ seems to be the best initialization – it starts with the lowest initial error – it converges to the same reduced-model as the iteration that started with $\mathcal{S}_0^{\{1\}}$, and also in the same number of steps. $\mathcal{S}_0^{\{1\}}$ achieves this without the need for original poles. This numerical evidence suggests robustness of *IRKA-PH* to the extent that it is able to correct bad initializations. Indeed, *IRKA-PH* could be expected to be more robust and converge faster than the original *IRKA*, which typically exhibits fast convergence. The reasons are twofold. First, unlike *IRKA*, regardless of initialization, every intermediate reduced model is stable; hence interpolation points never appear in the left-half plane. This smooths convergence behavior. Secondly, unlike *IRKA* which uses an oblique projector, *IRKA-PH* is theoretically equivalent to using an orthogonal projector (with respect to an inner product weighted by $\mathbf{Q}$).

For all these reasons, we expect *IRKA-PH* to be numerically robust and rapidly convergent. Throughout our numerical experiments using a wide variety of different initializations, we have *never* experienced a convergence failure of *IRKA-PH*. *IRKA-PH* always converged to the same reduced-model regardless of initialization; even a search for a counterexample spanning thousands of trials failed to produce even a single case of either convergence failure or convergence to a different model in the $r = 20$ case. Indeed this was true throughout the range $8 \le r \le 20$; *IRKA-PH* converged to the same reduced-model for many different initializations for $r = 8 : 2 : 20$. Only for $r = 2$, $r = 4$, and $r = 6$ and then only after several trials were we able to make *IRKA-PH* converge to a different reduced model. Indeed, only *one* different model emerged and it had only marginally better performance than the more easily found system.

We present one further comparison for the $r = 20$ case contrasting time domain simulations for full and reduced models. $\mathbf{G}$ has 2 inputs and 2 outputs. To make the time-domain illustrations simpler, we only compare the outputs of the subsystem relating the first input, u_1, to the first output, y_1. The results for the other 3 subsystems display the same behavior. As input, we choose a decaying sinusoid $u_1(t) = e^{-0.05t}\sin(5t)$ and run simulations for $T = 50$ s. The results are shown in Fig. 7. In Fig. 7(a), we plot the simulation results for the whole time interval. To give a better illustration, in Fig. 7(b), we zoom into the time interval [0, 10] s, showing that 1*StepIntrp* leads to the largest deviation. In Fig. 7(c), we give the absolute value of the error between the true system output and the reduced ones. As is clear from this figure and as expected from the earlier analysis as shown in Fig. 3, *IRKA* yields the smallest deviation. The maximum absolute values of the output errors, i.e. $\max|y_1(t) - y_{1,\mathrm{red}}(t)|$ where $y_{1,\mathrm{red}}(t)$ denotes the first output due to the reduced models are

IRKA-PH	1*StepIntrp*	*EffBal*
1.31×10^{-3}	1.09×10^{-2}	3.96×10^{-3}

6.2. MIMO port-Hamiltonian ladder network

As a second port-Hamiltonian system, we consider an n-dimensional ladder network as shown in Fig. 8. We take the current I on the left side and the voltage U on the right side of the ladder network as the inputs. The port-Hamiltonian outputs are the voltage over the first capacitor U_{C_1} and the current through the last inductor $I_{L_{n/2}}$. The state variables are as follows: x_1 is the charge

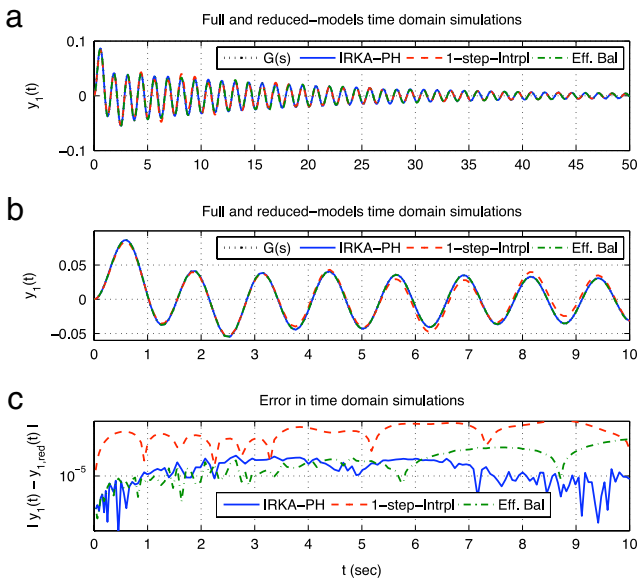

Fig. 7. Time domain simulations for mass–spring–damper system for $r = 20$.

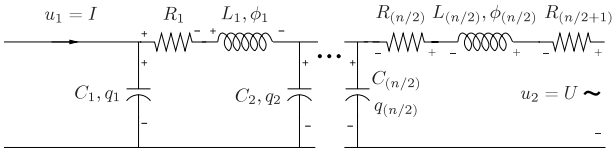

Fig. 8. MIMO ladder network.

q_1 of C_1, x_2 is the flux ϕ_1 of L_1, x_3 is the charge q_2 of C_2, x_4 is the flux ϕ_2 of L_2, etc. The directions chosen for the internal currents of the network are shown by plus- and minus-signs in Fig. 8. A minimal realization of this port-Hamiltonian ladder network for order $n = 4$ is given in Example 1. Adding another LC pair to the network, which would correspond to an increase of the dimension of the model by two, will modify the system matrices as follows: the subdiagonal of the matrix $\mathbf{A}$ will contain additionally $L_{n/2-1}^{-1}$, $-C_{n/2}^{-1}$ with the plus-sign in the $(n/2+1, n/2)$ position. The superdiagonal of $\mathbf{A}$ will contain $-C_{n/2}^{-1}$, $L_{n/2}^{-1}$ with the minus-sign in the $(n/2, n/2+1)$ position. Furthermore, the main diagonal of $\mathbf{A}$ will have $-\frac{R_{n/2-1}}{L_{n/2-1}}$ in the $(n-2, n-2)$ position, zero in the $(n-1, n-1)$ position, and $-\frac{R_{n/2}+R_{n/2+1}}{L_{n/2}}$ in the (n, n) position. The $\mathbf{B}$ matrix will be of the similar structure as in (15) with ones in the $(1, 1)$ and $(n, 2)$ positions and zeros in the rest.

We consider a 100-dimensional port-Hamiltonian network with $C_i = 0.1$, $L_i = 0.1$, and $R_i = 3$ for $i = 1, \ldots, 50$ and $R_{51} = 1$. For this model, we compare *IRKA-PH* to *EffBal*, *regular balanced truncation* (denoted by *RegBal*) and regular *IRKA*. Note that *RegBal* and *IRKA* do not preserve port-Hamiltonian structure. We include these methods in our comparisons to better illustrate the effectiveness of our proposed method. We show, for example, that *IRKA-PH* can perform as well as or sometimes better than *RegBal*, which is known to yield high-fidelity $\mathcal{H}_\infty$ and $\mathcal{H}_2$ performance (though it does not preserve port-Hamiltonian structure).

We reduce the order to $r = 1, 2, \ldots, 10$ (increments of one). The resulting relative $\mathcal{H}_2$ and $\mathcal{H}_\infty$ errors are shown in Fig. 9. The $\mathcal{H}_2$ character of our method is clear. *IRKA-PH* outperforms *EffBal* for every r. Interestingly, *IRKA-PH* is better than even *RegBal* for each $r = 1, \ldots, 5$. *RegBal* is better for $r = 6, 7, 8$, but for $r = 9, 10$, *IRKA-PH* is as good as *RegBal*. *IRKA-PH* achieves this performance while preserving structure and with no need to solve Lyapunov equations; the principal cost is sparse linear solves. *IRKA* yields the

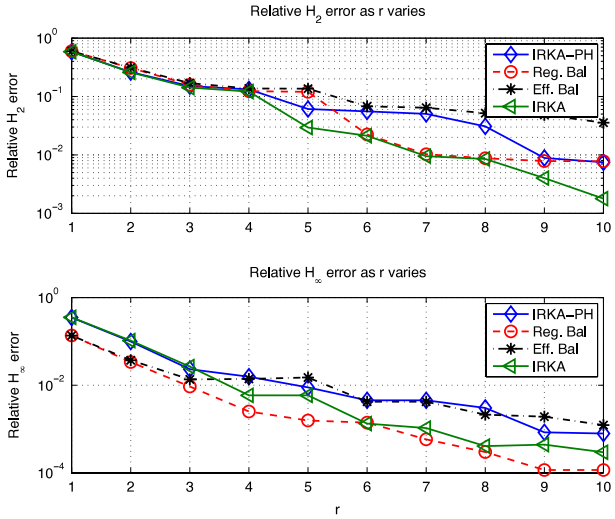

Fig. 9. Evolution of the relative $\mathcal{H}_2$ and $\mathcal{H}_\infty$ norms for ladder network.

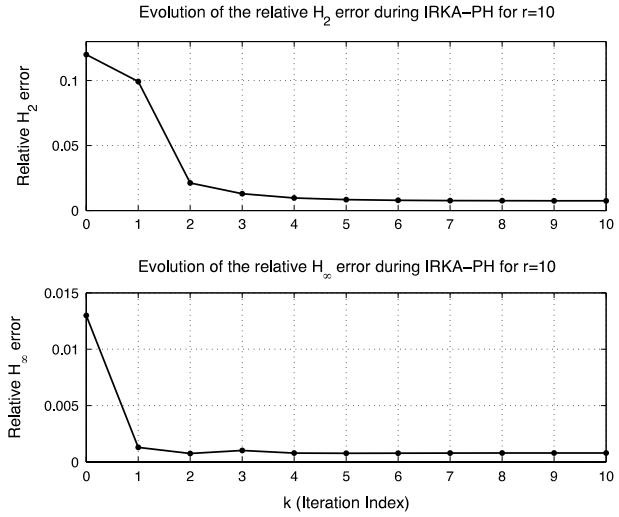

Fig. 10. Evolution of the relative $\mathcal{H}_2$ and $\mathcal{H}_\infty$ norms for ladder network for $r = 10$.

best $\mathcal{H}_2$ performance as it should, since it produces $\mathcal{H}_2$ optimal reduced-order models. *RegBal* is best in terms of $\mathcal{H}_\infty$ performance. Indeed, it is tailored towards $\mathcal{H}_\infty$ error reduction and is not constrained to preserve structure. However, the $\mathcal{H}_2$-based *IRKA-PH* performs as well as *EffBal* in terms of $\mathcal{H}_\infty$ error norm. This once more shows that, similar to *IRKA*, *IRKA-PH* provides high-fidelity not only in the $\mathcal{H}_2$ norm but also in the $\mathcal{H}_\infty$ norm.

Similar to the previous example, we illustrate the convergence behavior of *IRKA-PH*, in this case for $r = 10$, in Fig. 10. In this case, the convergence is even faster than the previous example with the algorithm converging after five to six steps. For this model, we have initialized the interpolation points for *IRKA-PH* arbitrarily as logarithmically spaced points between 10^{-2} and 10^{1}. As before, the initial tangent directions are chosen as the leading right singular vector of $\mathbf{G}(s)$ evaluated at the chosen interpolation points.

As we did in the previous example, we experiment with different initialization strategies for *IRKA-PH*. For brevity, we only illustrate the $r = 10$ case. We consider 5 different initializations, $\mathcal{S}_0^{\{j\}}$ for $j = 1, \ldots, 5$ for the interpolation points. $\mathcal{S}_0^{\{1\}}$ is what we used earlier. For $\mathcal{S}_0^{\{2\}}$, we choose $r = 10$ original system poles and perturb them by 0.1% as the starting points. This is a very poor choice since the interpolation points are very close to the system poles. For $\mathcal{S}_0^{\{3\}}$, we choose 10 points logarithmically spaced between -10^{-5} and -10^{-1}. Once again, these interpolation points

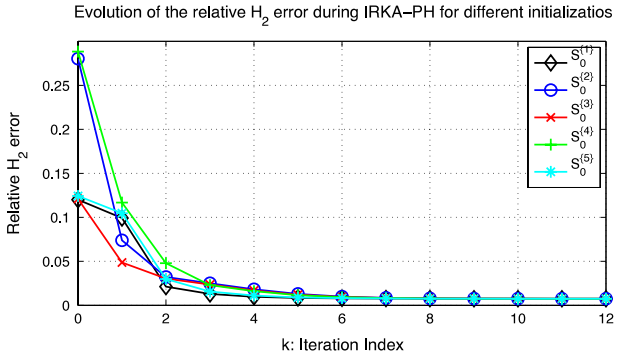

Fig. 11. Relative $\mathcal{H}_2$ norms for different initializations for ladder network for $r = 10$.

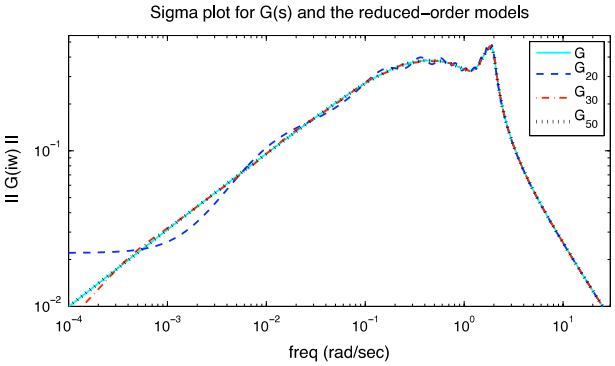

Fig. 12. Sigma plots of $\mathbf{G}(s)$ and the reduced models for mass–spring–damper system with $n = 20\,000$.

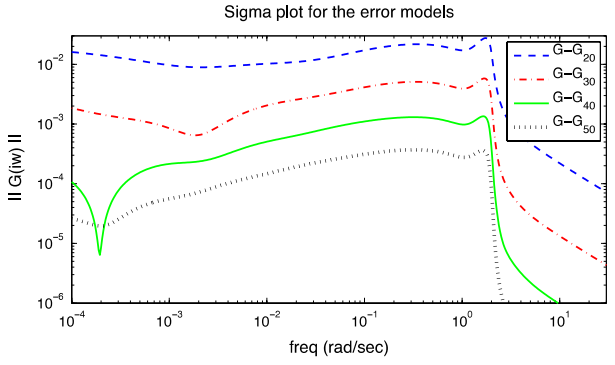

Fig. 13. Error sigma plots for mass–spring–damper system with $n = 20\,000$.

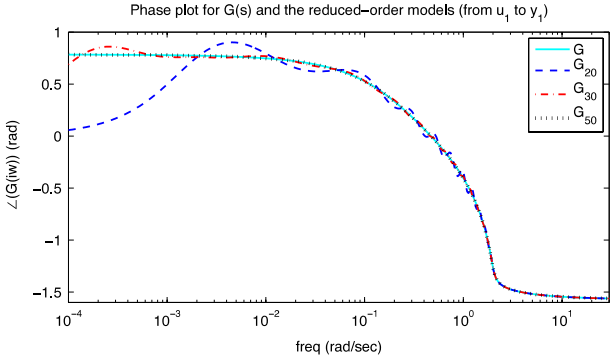

Fig. 14. Phase plots of $\mathbf{G}$ and the reduced models for mass–spring–damper system with $n = 20\,000$.

are also in the left-half plane; a strategy one would usually avoid. $\mathcal{S}_0^{\{4\}}$ correspond to choosing 10 points logarithmically spaced between 10^{-8} and 10^{-4}. And finally, for $\mathcal{S}_0^{\{5\}}$, we choose some arbitrary complex numbers where the real parts are distributed between 10^{-5} and 10^{-2} and the imaginary parts are distributed between 10^{-2} and 10^{0} together with their complex conjugate pairs. Once the starting points are chosen, the corresponding directions are the dominant right singular vectors of the transfer function at each interpolation point. Fig. 11 shows the evolution of the relative $\mathcal{H}_2$ error during *IRKA-PH* for these 5 different selections. As before, in all five cases, *IRKA-PH* converges to the same reduced-model in almost the same number of steps illustrating the robustness of *IRKA* to different initializations.

6.3. Mass–spring–damper system with $n = 20\,000$

In the previous two examples, to have a thorough analysis of the models with as many system norm computations as possible, we have chosen a very modest system size of 100. In this example, to illustrate that we can effectively apply our method in large-scale settings, we modify the mass–spring–damper model to have a full model of order $n = 20\,000$. Then, using *IRKA-PH*, we reduce the order to $r = 20$, $r = 30$ $r = 40$ and $r = 50$. In each case, the initial interpolation points are chosen as logarithmically spaced points between 10^{-3} and 10^{-1} with the corresponding tangential directions chosen as the leading singular vectors of the transfer function at these points. Before we present the results, we note that even at this scale, the method took less than one minute to converge with a rather straightforward implementation in Matlab. We have not tried to optimize the performance; we have simply used the Matlab sparse linear solves as is. The algorithm is expected to perform faster with the appropriate optimization of the code.

The sigma plots, i.e. $\|\mathbf{G}(\imath\omega)\|_2$ vs. ω, of the full-order model $\mathbf{G}(s)$ and three of the four reduced models are plotted in Fig. 12. We omitted the 40th order approximation to simplify the figure as the $r = 40$ approximation was visually indistinguishable from the $r = 50$ one. Except the $r = 20$ case, all the reduced models provide a high quality approximation to the full-order model of order $n = 20\,000$. To illustrate the approximation quality further, we display sigma plots of the error models in Fig. 13. As r increases, the quality of the approximation improves consistently; for $r = 50$, we obtain an *approximate*[2] relative $\mathcal{H}_\infty$ error of 7.90×10^{-4}. Hence, with the proposed algorithm, we are able to reduce a port-Hamiltonian system of order $n = 20\,000$ in a numerically effective structure-preserving way using interpolation. Moreover, with the $\mathcal{H}_2$-inspired interpolation point and tangential direction selection, the reduced-model of order $r = 50$ is accurate to a relative error of 7.90×10^{-4}.

The phase plots of the original model $\mathbf{G}(s)$ and the three of the four reduced-models are shown in Fig. 14. Once again we have left the 40th order approximation out due to the same reason as before. To make the figure simpler, we only show the phase plot of the subsystems relating the first input $(u_1(t))$ to the first output $(y_1(t))$. Similar to the sigma plot, Fig. 14 illustrates that plots for the full model $\mathbf{G}$ and for the reduced model $\mathbf{G}_{40}$ and $\mathbf{G}_{50}$ are virtually indistinguishable. $\mathbf{G}_{30}$ shows some deviations around the low frequencies (as in the sigma plot). And as expected, $\mathbf{G}_{20}$ has the largest deviation. The phase plots for the other 3 subsystems have a similar pattern and are omitted for brevity.

We conclude this example by illustrating time domain simulations for the same subsystem as above (from the first input $u_1(t)$ to the first output $y_1(t)$). We plot the results only for $\mathbf{G}$, $\mathbf{G}_{20}$ and

[2] We use the term *approximate* since both $\|\mathbf{G}\|_{\mathcal{H}_\infty}$ and $\|\mathbf{G}-\mathbf{G}_{50}\|_{\mathcal{H}_\infty}$ are computed by 500 frequency sampling points over the imaginary axis as opposed to an exact $\mathcal{H}_\infty$ norm computation. However, since the error plot is smooth, we expect this error number to be accurate enough.

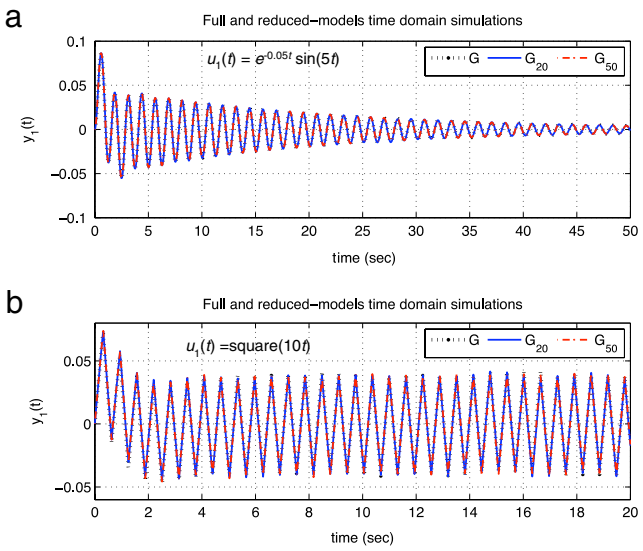

Fig. 15. Time domain simulations for mass–spring–damper system with $n = 20\,000$.

$\mathbf{G}_{50}$ to make the illustrations more readable. First we use a decaying exponential $u_1 = e^{-0.05t}\sin(5t)$ and run all three models for $T = 50$ s. The simulations are run using the Matlab ode45 solver (taking advantage of the sparsity of the matrices in the full-order simulations). The results are shown in Fig. 15(a). Both reduced-models follow the full-order output very accurately. The maximum value of the absolute errors in the output responses are 1.32×10^{-3} for $\mathbf{G}_{20}$ and 6.15×10^{-5} for $\mathbf{G}_{50}$. Accurate approximations are obtained in a fraction of the time, indeed. While the full-order simulation took 4.62 s, the reduced-order simulations took 0.066 s for $\mathbf{G}_{20}$ and 0.068 s for $\mathbf{G}_{50}$; more than 98% reduction in simulation time. Of course, these gains will be significantly magnified when the full-order model needs to be simulated over and over again for different input selections. The second input we try is a square wave that oscillates between 1 and -1 with a period of 0.2π s for the time interval 0–20 s. Fig. 15(b) shows the corresponding outputs. Once more, both reduced models display a high-fidelity match. For this second input, the max value of the absolute errors in the output responses are 7.38×10^{-3} for $\mathbf{G}_{20}$ and 5.85×10^{-3} for $\mathbf{G}_{50}$. Once again, the simulation of the reduced-order models took a fraction of the time that took the full-order simulation. The simulation for $\mathbf{G}$ took 9.15 s. On the other hand, it took 0.44 s for $\mathbf{G}_{20}$ and 0.46 s for $\mathbf{G}_{50}$; more than 95% reduction in simulation time. As the original system dimension increases even further, these gains in simulation times would be one of the biggest advantages of model reduction.

7. Conclusions

We have developed a framework for reducing multi-input/multi-output port-Hamiltonian systems via tangential rational interpolation. By choosing the projection subspaces appropriately, we obtain reduced-order models that are not only rational tangential interpolants of the original system but they also retain the original port-Hamiltonian structure. Thus, they are guaranteed to be passive. An $\mathcal{H}_2$-inspired algorithm is introduced for choosing the interpolation points and tangent directions for high-fidelity approximations. Several numerical examples show the effectiveness of the proposed method.

Acknowledgments

We would like to thank the anonymous referees for their valuable comments.

References

Antoulas, A. C. (2005). *Approximation of large-scale dynamical systems*. Society for Industrial and Applied Mathematics.

Antoulas, A. C., Beattie, C. A., & Gugercin, S. (2010). Interpolatory model reduction of large-scale dynamical systems. In J. Mohammadpour, & K. Grigoriadis (Eds.), *Efficient modeling and control of large-scale systems*. Springer-Verlag.

Beattie, C. A., & Gugercin, S. (2007). Krylov-based minimization for optimal $\mathcal{H}_2$ model reduction. In *46th IEEE conference on decision and control* (pp. 4385–4390).

Beattie, C. A., & Gugercin, S. (2009a). A trust region method for optimal $\mathcal{H}_2$ model reduction. In *Proceedings of the 48th IEEE conference on decision and control*.

Beattie, C. A., & Gugercin, S. (2009b). Interpolatory projection methods for structure-preserving model reduction. *Systems & Control Letters*, *58*(3), 225–232.

Benner, P., Quintana-Ortí, E. S., & Quintana-Ortí, G. (2003). State-space truncation methods for parallel model reduction of large-scale systems. *Parallel Computing*, *29*, 1701–1722. special issue on "Parallel and Distributed Scientific and Engineering Computing".

Bunse-Gerstner, A., Kubalinska, D., Vossen, G., & Wilczek, D. (2010). $\mathcal{H}_2$-norm optimal model reduction for large scale discrete dynamical MIMO systems. *Journal of Computational and Applied Mathematics*, *233*(5), 1202–1216.

De Villemagne, C., & Skelton, R. E. (1987). Model reductions using a projection formulation. *International Journal of Control*, *46*(6), 2141–2169.

Freitas, F. D., Rommes, J., & Martins, N. (2008). Gramian-based reduction method applied to large sparse power system descriptor models. *IEEE Transactions on Power Systems*, *23*(3), 1258–1270.

Gallivan, K., Vandendorpe, A., & Van Dooren, P. (2005). Model reduction of MIMO systems via tangential interpolation. *SIAM Journal on Matrix Analysis and Applications*, *26*(2), 328–349.

Grimme, E. (1997). Krylov projection methods for model reduction. Ph.D. Thesis. Coordinated Science Laboratory, University of Illinois at Urbana-Champaign.

Gugercin, S. (2005). An iterative rational Krylov algorithm (IRKA) for optimal $\mathcal{H}_2$ model reduction. In *Householder symposium XVI*, Seven Springs Mountain Resort, PA, USA.

Gugercin, S., Antoulas, A., & Beattie, C. (2006). A rational Krylov iteration for optimal $\mathcal{H}_2$ model reduction. In *Proceedings of MTNS. Vol. 2006*.

Gugercin, S., Antoulas, A. C., & Beattie, C. A. (2008). $\mathcal{H}_2$ model reduction for large-scale linear dynamical systems. *SIAM Journal on Matrix Analysis and Applications*, *30*(2), 609–638.

Gugercin, S., Polyuga, R. V., Beattie, C. A., & van der Schaft, A. J. (2009). Interpolation-based $\mathcal{H}_2$ Model Reduction for port-Hamiltonian systems. In *Proceedings of the joint 48th IEEE conference on decision and control and 28th Chinese control conference* (pp. 5362–5369).

Gugercin, S., Sorensen, D. C., & Antoulas, A. C. (2003). A modified low-rank Smith method for large-scale Lyapunov equations. *Numerical Algorithms*, *32*(1), 27–55.

Halevi, Y. (1992). Frequency weighted model reduction via optimal projection. *IEEE Transactions on Automatic Control*, *37*(10), 1537–1542.

Hartmann, C. (2009). Balancing of dissipative Hamiltonian systems. In I. Troch, & F. Breitenecker (Eds.), *ARGESIM-reports: vol. 35. Proceedings of mathMod 2009, Vienna, February 11–13, 2009* (pp. 1244–1255). Vienna, Austria: Vienna Univ. of Technology.

Hartmann, C., Vulcanov, V.-M., & Schütte, Ch. (2010). Balanced truncation of linear second-order systems: a Hamiltonian approach. *Multiscale Modeling & Simulation*, *8*, 1348–1367.

Heinkenschloss, M., Sorensen, D. C., & Sun, K. (2008). Balanced truncation model reduction for a class of descriptor systems with application to the Oseen equations. *SIAM Journal on Scientific Computing*, *30*, 1038.

Hyland, D., & Bernstein, D. (1985). The optimal projection equations for model reduction and the relationships among the methods of Wilson, Skelton, and Moore. *IEEE Transactions on Automatic Control*, *30*(12), 1201–1211.

Kubalinska, D., Bunse-Gerstner, A., Vossen, G., & Wilczek, D. (2007). H_2-optimal interpolation based model reduction for large-scale systems. In *Proceedings of the 16th international conference on system science*.

Meier, L., III, & Luenberger, D. (1967). Approximation of linear constant systems. *IEEE Transactions on Automatic Control*, *12*(5), 585–588.

Penzl, T. (2000). A cyclic low rank Smith method for large sparse Lyapunov equations. *SIAM Journal on Scientific Computing*, *21*(4), 1401–1418.

Polyuga, R. V. (2010). Model reduction of port-Hamiltonian systems. Ph.D. Thesis. University of Groningen.

Polyuga, R. V., & van der Schaft, A. J. (2008). Structure preserving model reduction of port-Hamiltonian systems. In *Proceedings of the 18th international symposium on mathematical theory of networks and systems*. Blacksburg, Virginia, USA, July 28–August 1. Publication available from http://sites.google.com/site/rostyslavpolyuga/publications.

Polyuga, R. V., & van der Schaft, A. J. (2010a). Model reduction of port-Hamiltonian systems as structured systems. In *Proceedings of the 19th international symposium on mathematical theory of networks and systems* (pp. 1509–1513).

Polyuga, R. V., & van der Schaft, A. J. (2010b). Structure preserving model reduction of port-Hamiltonian systems by moment matching at infinity. *Automatica*, *46*, 665–672.

Polyuga, R. V., & van der Schaft, A. J. (2011a). Structure preserving moment matching for port-Hamiltonian systems: Arnoldi and Lanczos. *IEEE Transactions on Automatic Control*, *56*(6), 1458–1462.

Polyuga, R. V., & van der Schaft, A. J. (2011b). Structure preserving port-Hamiltonian model reduction of electrical circuits. In P. Benner, M. Hinze, & J. ter Maten (Eds.), *Lecture notes in electrical engineering*, *Model reduction for circuit simulation* (pp. 241–260). Berlin, Heidelberg: Springer-Verlag.
Polyuga, R. V., & van der Schaft, A. J. (2012). Effort- and flow-constraint reduction methods for structure preserving model reduction of port-Hamiltonian systems. *Systems & Control Letters*, *61*(3), 412–421.
Sabino, J. (2007). Solution of large-scale Lyapunov equations via the block modified Smith method. Ph.D. Thesis. Rice University.
Sorensen, D. C., & Antoulas, A. C. (2002). The Sylvester equation and approximate balanced reduction. *Linear Algebra and its Applications*, *351*, 671–700.
Spanos, J. T., Milman, M. H., & Mingori, D. L. (1992). A new algorithm for L^2 optimal model reduction. *Automatica (Journal of IFAC)*, *28*(5), 897–909.
Stykel, T. (2004). Gramian-based model reduction for descriptor systems. *Mathematics of Control, Signals, and Systems (MCSS)*, *16*(4), 297–319.
The Geoplex Consortium, (2009). *Modeling and control of complex physical systems; the port-Hamiltonian approach*. Berlin, Heidelberg: Springer.
van der Schaft, A. J. (2000a). *L2-gain and passivity techniques in nonlinear control*. Springer-Verlag.
van der Schaft, A. J. (2000b). Port-controlled Hamiltonian systems: towards a theory for control and design of nonlinear physical systems. *Journal of the Society of Instrument and Control Engineers of Japan (SICE)*, *39*, 91–98.
van der Schaft, A. J., & Maschke, B. M. (1995). The Hamiltonian formulation of energy conserving physical systems with external ports. *Archiv für Elektronik und Übertragungstechnik*, *49*(5–6), 362–371.
van der Schaft, A. J., & Polyuga, R. V. (2009). Structure-preserving model reduction of complex physical systems. In *Proceedings of the joint 48th IEEE conference on decision and control and 28th Chinese control conference* (pp. 4322–4327).
Van Dooren, P., Gallivan, K. A., & Absil, P. A. (2008). $\mathcal{H}_2$-optimal model reduction of MIMO systems. *Applied Mathematics Letters*, *21*(12), 1267–1273.
Wilson, D. A. (1970). Optimum solution of model-reduction problem. *Proceedings of the Institution of Electrical Engineers*, *117*(6), 1161–1165.
Wolf, T., Lohmann, B., Eid, R., & Kotyczka, P. (2010). Passivity and structure preserving order reduction of linear port-Hamiltonian systems using Krylov subspaces. *European Journal of Control*, *16*(4), 401–406.
Yan, W. Y., & Lam, J. (1999). An approximate approach to h^2 optimal model reduction. *IEEE Transactions on Automatic Control*, *44*(7), 1341–1358.
Yousouff, A., & Skelton, R. E. (1985). Covariance equivalent realizations with applications to model reduction of large-scale systems. *Control and Dynamic Systems*, *22*, 273–348.
Yousuff, A., Wagie, D. A., & Skelton, R. E. (1985). Linear system approximation via covariance equivalent realizations. *Journal of Mathematical Analysis and Applications*, *106*(1), 91–115.
Zigic, D., Watson, L. T., & Beattie, C. (1993). Contragredient transformations applied to the optimal projection equations. *Linear Algebra and its Applications*, *188*, 665–676.

Serkan Gugercin is an Associate Professor in the Mathematics Department at Virginia Polytechnic Institute and State University, Blacksburg, VA, USA and a member of the Interdisciplinary Center for Applied Mathematics there. He received his B.S. degree in Electrical and Electronics Engineering in 1992 from Middle East Technical University, Ankara, Turkey; and his M.S. and Ph.D. degrees in Electrical Engineering from Rice University, Houston, TX, USA, in 1999 and 2003, respectively. His primary research interests include dynamical systems, scientific computation, and model reduction and control of large-scale systems. Dr. Gugercin received the Ralph Budd Award for Research in Engineering from Rice University, in 2003 for the best doctoral thesis in the School of Engineering; Teaching Award from Jacobs University Bremen, in 2003; and the National Science Foundation Early CAREER Award in Computational and Applied Mathematics in 2007. He is currently serving as an Associate Editor for Systems and Control Letters and for the IEEE Control Systems Society Editorial Board.

Rostyslav V. Polyuga graduated from Karazin Kharkiv National University, Ukraine, having obtained the Bachelor's degree in Applied Mathematics and Software Engineering (summa cum laude) in 2003, the Master's degree in Applied Mathematics and Software Engineering in 2004, and the Master's degree in Applied Economics in 2005. After working in industry as a Software Engineer in 2005, he joined the Johann Bernoulli Institute for Mathematics and Computer Science, University of Groningen, in 2006, where he defended his Ph.D. dissertation in Applied Mathematics in 2010. In March 2010 he was appointed as a postdoctoral researcher within the Centre for Analysis, Scientific Computing and Applications at the Department of Mathematics and Computer Science of Eindhoven University of Technology, where he carried out a joint project in numerical analysis for ASML Company. Since May 2011 he is with the Model Validation team of ABN AMRO Bank in Amsterdam.

Christopher Beattie is a Professor in the Mathematics Department at Virginia Tech and member of the Interdisciplinary Center for Applied Mathematics (ICAM) there. He has degrees from Duke University in Biomedical Engineering, Mechanical Engineering, and Computer Science; and a doctorate in Mathematical Sciences from Johns Hopkins University (1982). His principal research interests are in scientific computing and large scale computational linear algebra, with an emphasis on iterative Krylov methods. His primary focus is on model reduction of large scale dynamical systems with a goal of developing practical and rigorous computational algorithms for efficient manipulation and simulation of systems arising from physical models described by systems of partial differential equations.

Arjan van der Schaft (1955) received the undergraduate and Ph.D. degrees in Mathematics from the University of Groningen, The Netherlands, in 1979 and 1983, respectively. In 1982 he joined the Department of Applied Mathematics, University of Twente, Enschede, where he was appointed as a full professor in Mathematical Systems and Control Theory in 2000. In September 2005 he returned to Groningen as a full professor in Mathematics. He has served as Associate Editor for Systems and Control Letters, Journal of Nonlinear Science, SIAM Journal on Control, and the IEEE Transactions on Automatic Control. Currently he is Associate Editor for Systems and Control Letters, Journal of Geometric Mechanics, and Editor-at-Large for the European Journal of Control. Arjan van der Schaft is a Fellow of the Institute of Electrical and Electronics Engineers (IEEE).